



A simulation comparison of spatiotemporal and spatially-implicit size-structured models for northern shrimp and snow crab

Journal:	<i>Fish and Fisheries</i>
Manuscript ID:	Draft
Wiley - Manuscript type:	Original Article
Date Submitted by the Author:	n/a
Complete List of Authors:	Cao, Jie; North Carolina State University, Department of Applied Ecology Thorson, James; Alaska Fisheries Science Center, Habitat and Ecosystem Process Research Program Punt, André; University of Washington, School of Aquatic and Fishery Sciences Szuwalski, Cody; University of California, Santa Barbara, Bren School of Environmental Science and Management
Key terms:	spatio-temporal model, spatially-explicit stock assessment model, population spatial structure, Gaussian random fields, fishery selectivity
Abstract:	Characterizing population distribution and abundance over space and time is central to population ecology and conservation of natural populations. Exploited populations exhibit heterogeneous and complex spatial structure, and this heterogeneity is rarely modeled explicitly in resource assessments. However, population models that do not explicitly model spatial heterogeneity (called "spatially-implicit models" here) have several limitations, including the potential for vulnerability to exploitation ("selectivity") to vary among sizes/ages over time related to changing spatial distributions. We therefore develop a spatiotemporal model for estimating population dynamics at a fine spatial scale, demonstrated for two species with different types of life history, i.e., snow crab in the Eastern Bering Sea and northern shrimp in the Gulf of Maine. We compare the spatiotemporal model with a spatially-implicit model and systematically evaluate the spatiotemporal model based on simulation experiments. We show that the spatiotemporal model can recover spatial patterns in population and exploitation pressure as well as provide unbiased estimates of spatially-aggregated population quantities. The spatiotemporal models also implicitly account for individual movement rates, and can outperform spatially-implicit models by accounting for time-and-size varying selectivity caused by spatial heterogeneity. We therefore conclude that spatiotemporal modelling framework is a plausible and promising approach to address the spatial structure of natural resource populations, which is a major challenge in understanding population dynamics and conducting resource assessment and management.

SCHOLARONE™
Manuscripts

1
2 **A simulation comparison of spatiotemporal and spatially-implicit size-structured models for**
3 **northern shrimp and snow crab**

4

5 Jie Cao^{1,4*}, James T. Thorson², André E. Punt¹, Cody Szwalski³

6

7 1. School of Aquatic and Fishery Science, University of Washington, Seattle, WA 98195-5020,
8 USA

9 2. Fisheries Resources Assessment and Monitoring Division, Northwest Fisheries Science Center,
10 National Marine Fisheries Service, NOAA, 2725 Montlake Blvd. E, Seattle, WA 98112, USA
11 3. Bren School of Environmental Science and Management, University of California, Santa
12 Barbara, CA 93106, USA

13

14 Corresponding Author Email: jcao22@ncsu.edu

15

16 Present address

17 4. Department of Applied Ecology, Center for Marine Sciences and Technology, North Carolina
18 State University, Morehead City, NC 28557, USA

19

20 **Running Head:** Spatiotemporal size-structured model

21

22 **ABSTRACT**

23 Characterizing population distribution and abundance over space and time is central to
24 population ecology and conservation of natural populations. Exploited populations exhibit
25 heterogeneous and complex spatial structure, and this heterogeneity is rarely modeled explicitly in
26 resource assessments. However, population models that do not explicitly model spatial
27 heterogeneity (called “spatially-implicit models” here) have several limitations, including the
28 potential for vulnerability to exploitation (“selectivity”) to vary among sizes/ages over time related
29 to changing spatial distributions. We therefore develop a spatiotemporal model for estimating
30 population dynamics at a fine spatial scale, demonstrated for two species with different types of
31 life history, i.e., snow crab in the Eastern Bering Sea and northern shrimp in the Gulf of Maine.
32 We compare the spatiotemporal model with a spatially-implicit model and systematically evaluate
33 the spatiotemporal model based on simulation experiments. We show that the spatiotemporal
34 model can recover spatial patterns in population and exploitation pressure as well as provide
35 unbiased estimates of spatially-aggregated population quantities. The spatiotemporal models also
36 implicitly account for individual movement rates, and can outperform spatially-implicit models by
37 accounting for time-and-size varying selectivity caused by spatial heterogeneity. We therefore
38 conclude that spatiotemporal modelling framework is a plausible and promising approach to
39 address the spatial structure of natural resource populations, which is a major challenge in
40 understanding population dynamics and conducting resource assessment and management.

41

42 *Key words:* *spatio-temporal model; spatially-explicit stock assessment model; population spatial*
43 *structure; Gaussian random fields; fishery selectivity*

44 INTRODUCTION

45 Characterizing population distribution and abundance over space and time using
46 mathematical and statistical models is central to population ecology and the conservation of
47 terrestrial and aquatic organisms (Krebs 1972, Ehrlén and Morris 2015). These models include
48 species distribution models (e.g., Guisan et al. 2002, Elith and Leathwick 2009) that account for
49 abiotic and biotic covariates, and population dynamic models (Maunder and Piner 2015) that
50 estimate the amount of resource abundance and/or biomass (Bieber and Ruf 2005, Adams et al.
51 2008, Maunder and Piner 2015). These two types of model have fundamentally different structure,
52 so have rarely been integrated into a single modeling framework. As a result, natural resource
53 management and conservation measures are often developed based on simplifying assumptions
54 about, or implicit approximations to, population spatial structure, e.g., management of marine
55 fisheries resources (Goethel et al. 2011, Punt et al. 2015, Goethel and Berger 2017) and terrestrial
56 wildlife (Bieber and Ruf 2005, Adams et al. 2008). On the other hand, studies predicting effects
57 of environmental changes have focused primarily on species' distributions (Ehrlén and Morris
58 2015). A synthetic approach that simultaneously estimates abundance and distribution will
59 increase our ability to model complex populations, and therefore greatly improve natural resource
60 management and conservation.

61 The importance of considering population spatial structure has long been acknowledged
62 by fisheries scientists (e.g., Beverton and Holt 1957, Berkeley et al. 2004) and terrestrial ecologists
63 (Dunning et al. 1995, Turner et al. 1995). However, population ecology had primarily focused on
64 developing quantitative approaches to assess resource abundance while approximating dynamics
65 given the assumption that individuals are well mixed within the population spatial domain (i.e.,
66 spatial homogeneity). These approaches assume that population dynamics can be approximated by

67 tracking total abundance across the entire stock, including the classical Malthusian model of
68 exponential population growth, the Pearl-Verhulst model of logistic growth, and the Lotka-
69 Volterra models of population interactions. Models that do not explicitly model spatial
70 heterogeneity are hereinafter referred to as spatially-implicit models. Over the last two decades,
71 investigations into population spatial structure have been at the forefront of population ecology
72 (Jongejans et al. 2008, Goethel et al. 2011, Punt et al. 2015, 2016, Ehrlén and Morris 2015), due
73 in part to the lessons learned from management failures resulting from ignoring fine-scale
74 population spatial structure. There is extensive evidence suggesting that marine and terrestrial
75 populations are spatially patchy and locally structured (e.g., Elith and Leathwick 2009, Ehrlén and
76 Morris 2015, Boudreau et al. 2017).

77 Spatially-implicit population models are likely to yield biased estimates of population
78 quantities (Conroy et al. 1995, Turner et al. 1995, Sampson and Scott 2011, Goethel et al. 2015),
79 depending on the extent to which the underlying spatial structure of the population is mis-specified
80 (Punt et al. 2016). Spatially-stratified models have been developed to account for the emergent
81 spatial patterns caused by connectivity among subpopulations (Kareiva et al. 1990, Goethel et al.
82 2011, Chandler and Clark 2014). These models are typically structured using spatial strata and
83 explicitly model random (diffusive) and directed (migratory) movement of individuals among
84 strata (Okubo and Levin 1989, Kareiva et al. 1990). By estimating individual movement, spatially-
85 stratified models often require individual tagging data (Sippel et al. 2015), although spatial
86 capture-recapture models are increasingly proposed to estimate movement as well (Chandler and
87 Clark 2014, Chandler and Hepinstall-Cymerman 2016). Although these models address spatial
88 heterogeneity to some degree, challenges and limitations remain. First, correlations in process
89 errors (e.g., spatial patterns in juvenile survival) and anthropogenic impacts among spatial strata

90 are often ignored. Second, spatially-stratified models have typically not included any spatial
91 correlation among strata (either based on adjacency or distance). Therefore, the amount of data
92 per stratum decreases as the number of strata increases, such that spatially-stratified models have
93 typically included a small (2-10) number of spatial strata.

94 In marine system, local population processes are obscured, e.g., local depletion of weaker
95 subpopulation or persistent high fishing pressure on local concentrations, if fine-scale population
96 spatial structure is overlooked (Benson et al. 2015, Boudreau et al. 2017), which may lead to
97 overexploitation of local fish populations. Locally depleted populations may not be easily
98 replenished by recolonization (Kuo et al. 2015, Boudreau et al. 2017). Fishing is likely to increase
99 spatial aggregation potential due to size-selective harvest (Kuo et al. 2015). Therefore, spatial
100 patterns of both population density, productivity, and fishing pressure need to be evaluated to
101 prevent overfishing more vulnerable local subpopulations. Most population models that attempt to
102 capture spatial structure in fished populations underuse the available spatial information because
103 they are fit to abundance index, fisheries catch, and size- or age-compositions that are aggregated
104 spatially. By doing so, population and fishery processes (e.g., density-dependence, fishing pressure
105 and selectivity) and productivity are approximated as being homogeneous across the population
106 spatial domain (spatially-implicit models) or within a stratum (spatially-stratified models).
107 Therefore, variation in survey data among sampling locations is typically attributed to sampling
108 error, while some portion of this variation actually represents predictable spatial heterogeneity
109 (e.g., Thorson and Haltuch 2018).

110 Our objective was to link species distribution and population dynamic models within a
111 single statistical framework that is flexible enough to permit inference for each state variable (e.g.,
112 abundance and fishing mortality) through space and time. To do this, we build upon recent research

113 combining fish population dynamics and spatio-temporal statistics (Kristensen et al. 2014, Thorson
114 et al. 2015). Statistical methods and computational approaches for spatiotemporal models have
115 seen tremendous advances in recent years (Cressie et al. 2009). It is increasingly possible to fit a
116 spatiotemporal population model directly to available fishery and survey data, assuming that
117 population density varies continuously across space (Kristensen et al. 2014). We also structure the
118 population by size bins because most exploited species are size-truncated, and they tend to have
119 different spatial distributions among size/age classes (Lee et al. 2017), and because these size-
120 structured models are capable of discriminating between spatial heterogeneity in juvenile
121 production (called “recruitment”) and adult growth and survival (Thorson et al. 2015). Our model
122 addresses an important challenge in understanding fish population dynamics and conducting stock
123 assessment and management, i.e., the spatial structure of fish population and fisheries.

124 We first describe the general elements of the modeling framework mathematically and
125 show how, with straightforward modifications to the population dynamic component, it can
126 accommodate a wide range of species with various types of life history. We illustrate the
127 framework for two exploited marine species, i.e., snow crab (*Chionoecetes opilio*) in the Eastern
128 Bering Sea and northern shrimp (*Pandalus borealis*) in the Gulf of Maine, which have different
129 types of life history. We then use theoretical and simulation examples to demonstrate model
130 performance. This includes showing that the model: 1) can recover spatial patterns in population
131 and fishing pressure as well as provide unbiased estimates of spatially-aggregated population
132 quantities, 2) implicitly accounts for movement processes, and 3) outperforms spatially-implicit
133 models when population density and fishing pressure is spatially heterogenous.

134 **METHODS**

135 **Model development**

136 We present a size-structured spatiotemporal model, which estimates spatiotemporal
137 dynamics of size-structured populations and fisheries. To do so, we first describe a data model
138 linking observed data and its associated variation to latent population and fishery processes. The
139 data model combines inference on encounter probability and abundance. We then outline process
140 models describing the underlying population and fishery processes. Finally, we outline the
141 parameters of the proposed models, and how the estimation of these parameters and other derived
142 quantities is conducted. We represent matrices with bold uppercase notation, and vectors with bold
143 lowercase notation. Indices used in model descriptions, data used during parameter estimation and
144 simulation, and all parameters are listed in Table 1.

145 *Data model*

146 Understanding species population dynamics usually requires ecologists to collect data from
147 biological surveys, where sampling occurs at pre-defined sites, the amount of each species (counts
148 or biomass) is recorded, and the sampled animals are subsampled to collect more biological
149 information (e.g., maturity, sex, age and size). We let $x(s_i, t_i)$ represent i th observed count or
150 biomass of a species sampled at a site indexed by the spatial location s_i within a study area S ,
151 during time $t_i \in \{1, \dots, T\}$. The sampling locations are sometimes outside species' occupied habitat.
152 We therefore account for encounter probability in the observation model. The observation model
153 depends on the nature of the sampled data. For continuous data with zeros, i.e., biomass samples,
154 we represent the relationships among observed biomass catch rate at location s_i at time t_i , $x(s_i, t_i)$
155 , predicted biomass catch rate at location s_i at time t_i , $b(s_i, t_i)$, true local density of individuals,
156 $n(s_i, t_i)$, and encounter probability, $p(s_i, t_i)$, using a “Poisson-link” model, which overcomes
157 theoretical problems with the conventional delta models, and is more biologically interpretable
158 (Thorson 2017). The encounter probability is a function of local density:

159
$$p_i = 1 - \exp(-a_i n(s_i, t_i)) \quad (1)$$

160 where a_i is the area swept for sample i , which is taken at location s_i and time t_i , where the number
 161 of observed individuals follows a Poisson process with expectation $n(s_i, t_i)$ that is modeled in
 162 process model. Encounter probability p_i is therefore modeled with a complementary log-log
 163 (cloglog) link function given log-abundance density $\log(n(s_i, t_i))$. The cloglog-link is being
 164 increasingly used in other species distribution models (Phillips et al. 2017).

165 Predicted biomass catch rate when the species is encountered is then calculated as a product
 166 of density in numbers, $n(s_i, t_i)$, area swept a_i , and predicted biomass per group of individuals, δ
 167 (s_i, t_i):

168
$$b_i = \frac{a_i n(s_i, t_i) \times \delta(s_i, t_i)}{p_i} \quad (2)$$

169 The probability density function for biomass sample x_{s_i, t_i} is defined as:

170
$$\Pr(B = x_{s_i, t_i}) = \begin{cases} 1 - p_i & \text{if } x_{s_i, t_i} = 0 \\ p_i \times g(B; b_i, \sigma_D^2) & \text{if } x_{s_i, t_i} > 0 \end{cases} \quad (3)$$

171 where b_i and σ_D^2 are the mean and variance of B and the probability density function $g(B)$ can be
 172 lognormal or gamma. The lognormal distribution is used for catch rate data with no zero
 173 observations.

174 The observation model assumed for discrete count data is the overdispersed lognormal
 175 Poisson process:

176
$$\Pr(N = x_{s_i, t_i}) = \text{Poisson}(N; n(s_i, t_i) \times \exp(\eta_i)) \quad (4)$$

177 where x_{s_i, t_i} in this case is an observed count, and η_i is an observation-level random effect, which
 178 follows a normal distribution representing lognormal overdispersion.

179 Spatially-referenced fisheries-dependent data, i.e., total amount of fish by size class
 180 removed from the ocean, which are collected directly from the commercial and recreational

181 fisheries are used to estimate the spatial pattern of fisheries. The total catch by area/size is assumed
 182 to be lognormally distributed. The equations for calculating predicted catch are discussed later.

183 *Process model*

184 The process model is a spatiotemporal size-structured population model of abundance,
 185 where $n_{s,t}(l)$ is the density (abundance per area) at location s , time t , and size-class l , and we
 186 define $\mathbf{n}_{s,t} = (n_{s,t}(1), n_{s,t}(2), \dots, n_{s,t}(L))^T$. In general, we express the abundance $\mathbf{n}_{s,t+1}$ as a
 187 product of a function $g(\mathbf{n}_{s,t})$ and a process error term $e^{\boldsymbol{\varepsilon}_{s,t}}$:

$$188 \quad \mathbf{n}_{s,t+1} = g(\mathbf{n}_{s,t}) \circ e^{\boldsymbol{\varepsilon}_{s,t}} \quad (5)$$

189 where $\mathbf{n}_{s,t}$ is a vector of abundances for each of L size classes, and we use \circ to indicate the
 190 elementwise product of two vectors. $g(\mathbf{n}_{s,t})$ is a potentially nonlinear function of the previous
 191 abundance intensity and model parameters that describe the population dynamics. This function is
 192 general and can be chosen to match the life history of the species concerned. $\boldsymbol{\varepsilon}_t$ is a vector of
 193 random effects that implicitly accounts for unmodeled spatial and temporal processes, e.g.,
 194 movement, and spatial variation in biological parameters such as growth and natural mortality.

195 Process errors are assumed to follow a multivariate normal distribution:

$$196 \quad \mathbf{E}_t \sim \text{MVN}(0, \mathbf{R}_{\text{spatial}} \otimes \boldsymbol{\Theta}_L) \quad (6)$$

197 where \otimes denotes the Kronecker operator, $\boldsymbol{\Theta}_L$ is a L by L matrix of the pairwise variance-
 198 covariance between any two size classes, and $\mathbf{R}_{\text{spatial}}$ is a Matérn correlation matrix, where the
 199 pairwise correlation between two locations s_i and $s_i + h$ is:

$$200 \quad \mathbf{R}_{\text{spatial}}(s_i, s_i + h) = \frac{1}{2^{v-1}\Gamma(v)} \times (\kappa|h|)^v \times K_v(\kappa|h|) \quad (7)$$

201 where $\Gamma()$ is the gamma function, K_ν is the modified Bessel function, κ is the parameter governing
202 the distance h at which two locations are effectively uncorrelated, and ν is the Matérn smoothness
203 parameter which we fix at $\nu = 2$ for computational reasons (as discussed later).

204 We consider two population dynamics models: one for invertebrates that exhibit an
205 effective cessation of growth at some stage in the life history, and a general model that can be used
206 for fish and invertebrate which do not exhibit cessation of growth. Eastern Bering sea snow crab
207 and Gulf of Marine northern shrimp are used as examples of the two population dynamic types,
208 respectively.

209 *Example 1: Eastern Bering sea snow crab*

210 As a first example, we model abundance of snow crab in the Eastern Bering Sea. Snow
211 crab are distributed on the continental shelf of the Bering Sea and are common at depths less than
212 200 m. The U.S pot fishery began in the 1970s after the Japanese started harvesting them in the
213 1960s (but were subsequently excluded from the fishery in the early 1980s). The fishery peaked
214 in the 1990s and crashed in the 2000s. This species is one of the most important crab species in
215 terms of volume landed and value (Abbott et al. 2010). Research has shown that spatial dynamics
216 of the snow crab is likely affected by environmental effects, e.g., water temperature and sea ice
217 extent (Mueter and Litzow 2008, Parada et al. 2010).

218 We model the population dynamics by sex and maturity state because males and females
219 experience different fishing mortality rates (f) (only males are retained by the fishery) and they
220 cease growth when they reach sexual maturity. The size-specific abundance density over time is
221 controlled by recruitment ($\mathbf{r}_{s,t}$, a vector of length L representing the number of juvenile recruits
222 into each size class of the modelled population), growth (\mathbf{G} , a sex-specific matrix describing the
223 proportion of individuals staying in the same size class or growing into other size classes), natural

224 mortality (**m**), and fishing mortality (*f*). We express $g(\mathbf{n}_{s,t})$ by sex indicated by superscripts male
225 and female as:

$$226 \quad g(\mathbf{n}_{s,t}^{\text{male}}) = \\ 227 \quad \begin{cases} \mathbf{r}_{s,t} p^{\text{male}} + \mathbf{G}^{\text{male}}(\mathbf{n}_{s,t-1}^{\text{male}} \circ \exp(-\mathbf{m}_{s,t-1} - \mathbf{v}f_{s,t-1}^{\text{male}})) \circ (1 - \mathbf{w}^{\text{male}}), & \mathbf{n} = \mathbf{n}^\lambda \\ \mathbf{G}^{\text{male}}(\mathbf{n}_{s,t-1}^{\text{male}} \circ \exp(-\mathbf{m}_{s,t-1} - \mathbf{v}f_{s,t-1}^{\text{male}})) \circ \mathbf{w}^{\text{male}} + \mathbf{n}_{s,t-1}^h \circ \exp(-\mathbf{m}_{s,t-1} - \mathbf{v}f_{s,t-1}^{\text{male}}), & \mathbf{n} = \mathbf{n}^\omega \end{cases} \quad (8)$$

$$229 \quad g(\mathbf{n}_{s,t}^{\text{female}}) = \\ 230 \quad \begin{cases} \mathbf{r}_{s,t}(1 - p^{\text{male}}) + \mathbf{G}^{\text{female}}(\mathbf{n}_{s,t-1}^{\text{female}} \circ \exp(-\mathbf{m}_{s,t-1})) \circ (1 - \mathbf{w}^{\text{female}}), & \mathbf{n} = \mathbf{n}^\lambda \\ \mathbf{G}^{\text{female}}(\mathbf{n}_{s,t-1}^{\text{female}} \circ \exp(-\mathbf{m}_{s,t-1})) \circ \mathbf{w}^{\text{female}} + \mathbf{n}_{s,t-1}^h \circ \exp(-\mathbf{m}_{s,t-1}), & \mathbf{n} = \mathbf{n}^\omega \end{cases} \quad (9)$$

231 where superscripts λ and ω indicate maturity and immaturity, respectively, **w** is a vector
232 representing the proportion w_l of immature individuals at length *l* that mature, p^{male} is the sex ratio
233 of the recruits, **m** is a vector of natural mortality, *f* is fully selected fishing mortality, and **v** is a
234 vector of selectivity coefficients.

235 We complete this dynamical model by specifying how male and female abundance is
236 initialized in the first modeled year:

$$237 \quad g(\mathbf{n}_{s,1}^{\text{male}}) = \mathbf{r}_{s,1} p^{\text{male}} \circ \exp(\boldsymbol{\varphi}_{\text{male}}) \quad (10)$$

$$238 \quad g(\mathbf{n}_{s,1}^{\text{female}}) = \mathbf{r}_{s,1}(1 - p^{\text{male}}) \circ \exp(\boldsymbol{\varphi}_{\text{female}}) \quad (11)$$

239 where $\boldsymbol{\varphi}_{\text{male}}$ and $\boldsymbol{\varphi}_{\text{female}}$ are vectors representing abundance at size of the first modeled year for
240 males and females, respectively. These abundances at size are assumed constant across the study
241 area. This model assumes that females are not fished (i.e., $f_{s,t-1}^{\text{female}} = 0$) given that discard mortality
242 of females is very low (Szwalski and Punt 2015).

243 Spatially-referenced fishery data (catch-at-size) are included in the likelihood function. The
244 predicted harvest per area removed by the fishery, **c**_{s,t}, for snow crab is calculated as:

$$245 \quad \mathbf{c}_{s,t} = (1 - \exp(-\mathbf{v}f_{s,t}^{\text{male}})) \circ \mathbf{n}_{s,t}^{\text{male}} \circ \exp(-0.5\mathbf{m}_{s,t}) \quad (12)$$

246 This catch equation implicitly assumes that fishing during year t takes place rapidly at the middle
 247 of the year because the fishery for male snow crab is considered to take place as a pulse.

248 *Example 2: Gulf of Maine northern shrimp*

249 As a second example, we model abundance of northern shrimp in the Gulf of Maine. The
 250 Gulf of Maine marks the southern-most extent of the species' range. Therefore, this population is
 251 sensitive to ocean temperature changes. The population is estimated at the lowest level ever and
 252 has experienced failed recruitment for the past several years (Cao et al. 2017). As a result, the
 253 fishery has been closed since the 2014 fishing season. Projections suggest that the stock is unlikely
 254 to recover due to warming temperature, low recruitment and high natural mortality.

255 Here sex is not distinguished because northern shrimp are hermaphroditic, so we specify $g($
 256 $\mathbf{n}_{s,t})$ for both males and females as:

$$257 \quad g(\mathbf{n}_{s,t}) = \mathbf{G}(\mathbf{n}_{s,t-1} \circ \exp(-\mathbf{m}_{s,t-1} - \mathbf{v}f_{s,t-1})) + \mathbf{r}_{s,t} \quad (13)$$

258 and initialize abundance using

$$259 \quad g(\mathbf{n}_{s,1}) = \mathbf{r}_{s,1} \circ \exp(\boldsymbol{\varphi}) \quad (14)$$

260 These abundances at size are assumed constant across the study area.

261 The predicted catch per area, $\mathbf{c}_{s,t}$, for northern shrimp is calculated using the Baranov catch
 262 equation assuming natural and fishing mortality take place continuously over a modeled time unit:

$$263 \quad \mathbf{c}_{s,t} = \frac{\mathbf{v}f_{s,t}}{\mathbf{v}f_{s,t} + \mathbf{m}_{s,t}} \circ (1 - \exp(-\mathbf{m}_{s,t} - \mathbf{v}f_{s,t})) \circ \mathbf{n}_{s,t} \quad (15)$$

264 For both models, log-fishing mortality at each location in each year $\log(f_{s,t})$ is modeled
 265 as a random walk process given fishing mortality the previous year:

$$266 \quad \log(f_{s,t}) | \log(f_{s,t-1}) \sim N(\log(f_{s,t-1}), \sigma_f^2) \quad (16)$$

267 Size-specific selectivity is modeled using a logistic function of individual size, allowing the
268 probability of capture to vary with fish size:

269

$$v_l = \frac{1}{1 + e^{-\theta(d_l - l_{50})}} \quad (17)$$

270 where θ and l_{50} are the parameters of the logistic function and d_l is the midpoint of size-class l .

271 *Model parameters and estimation*

272 The spatial variation of recruitment, $\mathbf{r}_{s,t}$, is confounded with spatial process error (i.e.,
273 spatial variation in the abundance of each of the L size classes) if modeled separately (e.g., $r_{l,t} \sim$
274 $\text{MVN}(r_\mu \mathbf{R}_{\text{spatial}})$ where r_μ is the average recruitment at each location), because the size classes
275 used to define recruitment are included in L . We therefore allow spatial process error to account
276 for spatial variation in recruitment and estimate a set of average recruitment in each year (i.e., r_t).

277 In this case, $\mathbf{r}_{s,t}$ is equal to r_t for all locations s .

278 The parameters that are treated as fixed effects include process error covariance (Θ_L), the
279 parameter controlling the distance at which spatial correlations reach 10% (κ), average recruitment
280 for each time (r_t), initial abundance at size (φ), the selectivity parameters (θ and l_{50}), and the
281 standard deviations of fishing mortality and observations (σ_f and σ_D). We assume the growth
282 transition matrices \mathbf{G} , the proportion male at recruitment p_{male} , the proportion achieving maturity
283 at each size \mathbf{w} , and natural mortality rate for each size class \mathbf{m} are specified based on external
284 information (values used in this study are listed in Table A1 and A2). Future work could explore
285 estimating these parameters using additional data or meta-analytic information (e.g., Thorson et
286 al. 2017a).

287 We treat the fully-selected fishing mortality at each location over time (\mathbf{f}_s), and the
288 abundance for each size class and time (\mathbf{N}) as random effects. We treat abundance as a random

289 effect, rather than process error (\mathbf{E}_t), because this state-space parameterization leads to faster
 290 parameter estimation in a similarly structured model (Thorson et al. 2017c). To estimate the fixed
 291 effects, we maximize the marginal likelihood function after integrating across the random effects.
 292 We use Template Model Builder, TMB (Kristensen et al. 2015) called from within the R statistical
 293 environment (R Core Team, 2015) to do so. The detailed procedure of estimating parameters and
 294 uncertainty using TMB is described in Thorson et al. (2017b).

295 Computational issues arise when modeling spatiotemporal population dynamics as
 296 Gaussian Fields (GFs). Consequently, we use a stochastic partial differential equation
 297 approximation to the GF (i.e., Σ_t) based on a Gaussian Markov random field (GMRF) (Kristensen
 298 et al. 2015). This approach is based on a triangulation of the spatial domain, where a mesh is
 299 created based on a predefined number of nodes ('knots'). The number of knots determines the
 300 spatial resolution of the model, and is chosen as a trade-off between the accuracy of the GMRF
 301 representation and computational cost. The scale at which survey data were collected is not likely
 302 to coincide with the spatial scale of the model, i.e., the knots. Therefore, we model the abundance
 303 densities and use a "predictive process" formulation wherein we assume these function-valued
 304 variables are piecewise constant in the neighborhood of the knots. When calculating total
 305 abundance for year t , n_t , the densities at the modeled spatial locations are scaled up by the total
 306 area associated with the knots:

$$307 \quad n_t = \sum_{j=1}^J a_j \sum_{l=1}^L n_{l,j,t} \quad (18)$$

308 where $\mathbf{n}_{j,t}$ is the local density at knot j for each size class, a_j is the total area associated with knot
 309 j , and J is the number of knots specified. Fishery catch for each size class is aggregated at knot-
 310 level as input data. Therefore, total catch of year t , c_t , is calculated as:

$$311 \quad c_t = \sum_{j=1}^J \sum_{l=1}^L c_{l,j,t} \quad (19)$$

312 Simulation experiments

313 *Simulation overview*

We conducted three simulation experiments to (1) explore how the spatiotemporal model performs when individual movement processes are modeled explicitly, (2) compare spatially-implicit and spatiotemporal models, and (3) evaluate the impact of changing sample size. We developed two operating models (OMs) to simulate snow crab and northern shrimp populations, respectively. We use snow crab example to explore movement, the northern shrimp example to compare models, and both species to quantify the effect of sample size.

320 *Experiment 1: Exploring movement*

321 Simulation 1 is used to examine how model performance is affected by individual
322 movement processes that are modeled explicitly in the OM. Additionally, we evaluated whether
323 the spatiotemporal population model (1) captures the spatial structure and pattern in population
324 abundance and fishing mortality of each size class over time, and (2) provides unbiased estimates
325 of spatially-aggregated abundance and model parameters, such as fishery selectivity.

We developed an operating model to simulate a snow crab population and fishery in the eastern Bering Sea and generate data sets. We explicitly include movement in the OM to evaluate whether the estimation framework implicitly accounts for movement processes. Therefore, the process model in the OM is expressed as:

$$\mathbf{N}_{t+1} = g(\mathbf{M}\mathbf{N}_t) \circ e^{\Sigma_t} \quad (20)$$

331 where \mathbf{M} is a movement matrix (number of grid cells by number of grid cells) representing
 332 proportions of individuals that stay at their current location or move to other locations during a
 333 given time unit t , \mathbf{N}_t is an abundance matrix (number of grid cells by number of size classes).

334 Movement is assumed to occur at the start of each model time step. We derive annual \mathbf{M} from
335 instantaneous movement rates (Appendix 1). There is no movement when \mathbf{M} is an identity matrix.

336 We examined three scenarios: (1) the data are generated without measurement error and
337 there is no movement in the OM; (2) same as scenario 1, except there is movement; and (3) the
338 data have measurement error and there is movement in the OM.

339 To simplify the analysis, the OM only involves males for five size classes over 10 years.
340 However, we simulated the dynamics at a fine spatial scale, i.e., at each of 36,140 2 km by 2 km
341 grid cells that represent the area surveyed in the eastern Bering Sea bottom trawl survey.

342 Simulating the population and fishery dynamics involves the following steps: (1) specifying the
343 information used in the OM (summarized in Table A1); (2) simulating recruitment and fishing
344 mortality on the grids over time, $\mathbf{r}_{s,t}$ and $f_{s,t}$ (see Appendix 2 for detailed description); (3)
345 calculating the abundance of each size class $\mathbf{n}_{s,t}$ (using Eq. 6); and (4) applying annual movement
346 for scenarios 2 and 3. Thus, within one model time step, the OM tracks both dynamics occurring
347 within a single grid cell (i.e., survival, size transition and reproduction) and dynamics occurring
348 among grid cells (i.e., movement).

349 The OM can be readily modified to incorporate spatial variation in life history parameters,
350 e.g., grid-specific growth and natural mortality. However, for this study, we assume that spatial
351 variation in abundance is driven by spatial heterogeneity in fishing mortality, recruitment,
352 movement, and other space-and-size correlated processes are represented by process errors.
353 Fishing mortality in the OM is spatially-correlated, but this is not explicitly accounted for in the
354 estimation model (EM), which only includes temporal correlation. We specified 100 knots in the
355 EM (each one representing local densities simulated within 361 grid cells on average in the OM)
356 to approximate the fine-scale spatial processes simulated in the OM.

357 To generate the data sets from the OM, 200 sites (grid cells) in the OM were randomly
358 sampled each year. For each site, total abundance by size class and the total area of the sampled
359 site were recorded. Fishery catch-at-size was calculated at each of the 36,140 grids (using Eq. 10)
360 and then aggregated to the knot level as data for the EM. For the scenarios with measurement error,
361 we generated 100 replicated data sets with sampling errors, i.e., grid-based survey abundance and
362 fishery catch data were assumed to be lognormally distributed (see Appendix 3).

363 *Experiment 2: comparison of spatiotemporal and spatially-implicit models*

364 The intent of this experiment is to demonstrate the importance of accounting for spatial
365 processes when modeling the population dynamics of marine species. The spatially-implicit model
366 uses the same equations to describe the size-structured population dynamics as the spatiotemporal
367 model. However, it can only track the spatially-aggregated size-structured population over time.
368 Thus, it ignores all the spatial heterogeneities (i.e., all model variables are assumed to be constant
369 across space). The technical details of the spatially-implicit model can be found in Cao et al. (2017).
370 This model fits to spatially-aggregated data sets generated using the OM as described in Appendix
371 3.

372 This experiment is based on northern shrimp in the Gulf of Maine, and the spatial domain
373 of the population is the sampling domain of the northern shrimp summer survey in the western
374 Gulf of Maine (Cao et al. 2017). We simulate the size-structured population dynamics over 20
375 years on a grid with 4,997 2 km by 2 km cells over the spatial domain. The simulation procedure
376 is similar to the snow crab example, except $\mathbf{n}_{s,t}$ is calculated using Eq. 8 and movement is not
377 considered. The shrimp population and fishery are simulated to mimic the real world where the
378 recruitment is driven by temperature and stock size experienced a boom-and-bust circle (Table
379 A2; Cao et al. 2017). The fisheries mainly occur in inshore waters. Therefore, we simulate the

380 fishing mortality with the spatial structure so that inshore areas have consistently higher fishing
381 mortality over years (see Appendix 2).

382 Fifty simulated data sets are analyzed by the spatiotemporal and spatially-implicit models,
383 using the sampling process in Appendix 3. Each simulated data set includes survey catch rates by
384 size, with an intensity of 1,200 sampling tows (60 sampling locations per year) and catch-at-size
385 in all the grids for 20 years. To make a fair comparison, we ensure that, for each model iteration,
386 the data used in both estimation models are the same at the grid spatial scale (the input data for
387 spatially-implicit model are aggregated across grids, see Appendix 3 for details), and the values of
388 the pre-specified life history parameters (natural mortality and growth) are the same for the
389 spatiotemporal and spatially-implicit estimation models. We use 50 knots for the spatiotemporal
390 model. To assess model performance in this simulation experiment, we keep the replicates where
391 both estimation models converged (i.e., final gradient of the likelihood <0.001 and the Hessian of
392 fixed effects was positive definite). For converged replicates, we record all parameter estimates as
393 well as model predictions. We also record the number of non-converged runs.

394 The spatiotemporal model estimates population density for each of 50 knots, while the
395 spatially-implicit model estimates population abundance for the entire area. Therefore, to compare
396 results we convert results from the spatiotemporal model to a metric that is directly comparable
397 with the spatially-implicit model. To do so, we compare the estimates of abundance-at-size,
398 fishing mortality at size and spawning stock biomass aggregated over the spatial domain from both
399 models. The population-level fishing mortality f_t and aggregate selectivity-at-length $s_{l,t}$ for each
400 size class is determined by solving:

$$401 \quad c_{l,t} = (1 - \exp(-s_{l,t}f_t))n_{l,t} \exp(-m_t) \quad (21)$$

402 for a given value of catch $c_{l,t}$, abundance $n_{l,t}$, and natural mortality rate m_t , where $c_{l,t} = \sum_{j=1}^J c_{l,j,t}$
 403 and $n_{l,t} = \sum_{j=1}^J n_{l,j,t}$ are aggregated total catch and abundance for size class l and year t ,
 404 respectively. After solving for $s_{l,t}f_t$ for each year t and size l , we separately identify fishing
 405 mortality f_t and selectivity-at-length $s_{l,t}$ by defining $\text{argmax}_l(s_{l,t}) = 1$ for each year t : this
 406 definition of selectivity is common in fisheries stock assessment modelling (Sampson et al. 2011).
 407 Aggregate selectivity-at-size $s_{l,t}$ in the spatial operating or estimation model is not constrained to
 408 follow any parametric shape, even though local selectivity at length v_l follows a logistic function.
 409 In particular, aggregate selectivity-at-size $s_{l,t}$ will differ from local selectivity v_l whenever fishing
 410 mortality varies strongly among spatial locations (Sampson et al. 2011, Sampson and Scott 2012).

411 We finally compare the estimates with the true values and calculate the relative error in
 412 percentage for each year:

$$413 \quad e_{i,k} = \left(\frac{\text{est}_{i,k} - \text{true}_{i,k}}{\text{true}_{i,k}} \right) \times 100\% \quad (22)$$

414 where $\text{est}_{i,k}$ and $\text{true}_{i,k}$ are estimated and true values of i th model and k th replicate. We also
 415 calculate root-mean-square error (RMSE) and relative bias (RB) in percentage of estimated
 416 abundance at size across years:

$$417 \quad \text{RMSE}_l = \sqrt{\frac{\sum_t \left(\frac{n_{l,t}^{\text{est}} - n_{l,t}^{\text{true}}}{n_{l,t}^{\text{true}}} \right)^2}{\tau}} \times 100\% \quad (23)$$

$$418 \quad \text{RB}_l = \frac{\sum_t \left(\frac{n_{l,t}^{\text{est}} - n_{l,t}^{\text{true}}}{n_{l,t}^{\text{true}}} \right)}{\tau} \times 100\% \quad (24)$$

419 where $n_{l,t}^{\text{est}}$ and $n_{l,t}^{\text{true}}$ are the estimated and OM abundance of size class l in year t , and τ is the
 420 number of years.

421 *Experiment 3: Effect of sample size*

422 We finally conduct a systematic simulation experiment to evaluate model performance
423 given different sample sizes and provide some insight on the data requirements for the model to
424 have acceptable performance. We use both snow crab and northern shrimp as example species and
425 examine three levels of sampling intensity, i.e., 50, 100, and 200 locations per year, representing
426 data poor, moderate level, and data rich scenarios. We examine the model convergence rate (final
427 gradient of the likelihood <0.001) and root-mean-square error (RMSE) and relative bias (RB) in
428 percentage of estimated abundance at size across years for each scenario.

429 **RESULTS**430 **Experiment 1: Exploring movement**

431 The spatiotemporal model can generate unbiased and precise estimates of abundance and
432 fishing mortality spatially when data are not subject to measurement error and no movement occurs.
433 This confirms that the model is unbiased when correctly specified and when data are highly
434 informative as expected from maximum likelihood theory. A comparison between simulated and
435 estimated abundance shows how the spatiotemporal population model is able to reconstruct spatial
436 variation in abundance over time (Fig. 1). The general spatial pattern of each size class is recovered
437 by the EM (Fig. 1). However, the estimated spatial distribution misses some fine-scale patterns,
438 e.g., size class 3 in year 1 (Fig. 1). This is because the EM has a much coarser spatial resolution
439 than the OM (i.e., 100 knots to approximate 36,140 grid cells) and integrates over fine-scale
440 variation. As the number of knots increases, the estimated distribution would become smoother.
441 The estimated spatial distribution has lower total variation (reflected by the contrast in color) than
442 the true distribution. This is due to shrinkage, i.e., the estimate of abundance at a given location is
443 shrunk towards the average of its neighboring locations. The spatiotemporal model is able to

444 perfectly recover the spatial variation when the spatial scale at which data were collected and the
445 model operates matches (i.e., fishery catch data are aggregated to a knot-level, which matches the
446 model spatial scale) (Fig. A2). As a result, fully selected fishing mortality at the knot level is
447 unbiased through space and time (Fig. A3), and selectivity is also accurately estimated (i.e.,
448 estimated $\theta = 0.05$; $l_{50} = 75.15\text{mm}$). Accurate and precise estimates of abundance and catch are
449 also obtained when model outputs are aggregated spatially (Fig. 2). The 95% confidence intervals
450 are too tight to visualize (Fig. 2), suggesting that results are very precise when data are generated
451 without measurement error.

452 The model accounts for movement implicitly via its estimates of process error when the
453 spatiotemporal model fits to data without measurement error but generated given unmodeled
454 individual movement. The instantaneous movement rate applied in OM is 0.4yr^{-1} , i.e. about 35%
455 of crabs within a given grid in the OM move out every year. This unmodeled spatial process did
456 not lead to poorer model performance. The model recovers the spatial variation in abundance and
457 fishing mortality over time (Figs. A4 and A5), and the total abundance is estimated accurately
458 (Fig. A6). Finally, the spatiotemporal model converges (maximum gradient of the likelihood
459 <0.001) for all 100 simulation replicates when fitted to data given process error and individual
460 movement. The model is able to recover the spatial variation and accurately estimate the spatially-
461 aggregated abundance and catch with lower precision (Fig. 3), when the sampling errors are
462 present.

463 **Simulation experiment 2: Comparing spatially-implicit and spatiotemporal models**

464 The relative errors of estimated abundance-at-size suggest that the spatiotemporal model
465 outperforms the spatially-implicit model (Fig. 4). The relative errors of the spatiotemporal model
466 fluctuate around zero across years, where some of the years have relative errors centered around

467 zero and others have the median relative error below and above zero (Fig. 4; the median RMSE
468 across years are about 4% for all five size classes, and the RB are negative for the first three size
469 classes (-1.99%, -0.99%, -0.19%) and positive for the other two, i.e., 1.77%, 0.26%). The
470 spatiotemporal model always underestimates the abundance of all size-classes for years 9 and 18.
471 However, the spatially-implicit model produced biased estimates of abundance for all size classes
472 as none of the relative errors are centered around zero (the median RB are -5.93%, -5.65%, -5.35%,
473 -5.98%, and -11.27% for the five size classes, respectively). Almost all of the relative errors are
474 below zero, suggesting the spatially-implicit model consistently underestimates abundance-at-size.
475 As a result, the spatially-implicit model underestimates the total abundance and spawning stock
476 biomass for all years by about 10 to 20% (Fig. 5). The spatiotemporal model was able to estimate
477 the total abundance and spawning stock biomass relatively well for all years except year 18.

478 The comparison between estimated size-specific selectivity from the spatially-implicit
479 model and true population-level selectivity suggests that the underestimation of abundance is
480 likely due to biased estimates of aggregate selectivity (Fig. 6). The fishing mortality for size class
481 5 is greatly overestimated for most of the years. However, the spatiotemporal model was able to
482 estimate the population-level selectivity well (Fig. 6). Although selectivity in the OM is asymptotic
483 (i.e., a logistic curve), selectivity for some years suggests the spatially-aggregated population
484 selection from the spatial OM can be dome-shaped, e.g., years 8 and 16. This could be captured
485 by spatiotemporal model, but not the spatially-implicit model (Fig. 6).

486 **Experiment #3: Impact of changing sample sizes**

487 The convergence rate increases, the average relative error decreases, and the relative bias
488 approaches zero as the number of sampled locations increases from 50, 100, or 200 per year (Fig
489 7 for the two species). The convergence rates for northern shrimp are 68%, 72%, and 82% for the

490 data poor, data moderate and data rich scenarios, respectively. The corresponding convergence
491 rates for snow crab case are lower, i.e., 54%, 64%, and 74%. This might be due to the simulated
492 underlying spatial scale of snow crab being finer than that of northern shrimp (i.e., the total number
493 of grids used for snow crab simulation is about an order of magnitude greater than that used in
494 northern shrimp). The RMSE appears to decrease as the square-root of annual sample sizes as
495 predicted by maximum likelihood asymptotic theory (RMSE for northern shrimp: 6.1%, 3.9%, and
496 2.8%; RMSEs for snow crab: 3.8%, 2.8%, and 2.1%). The model performs worse for northern
497 shrimp than for snow crab (Table 2; Fig. 7). Also, the model slightly overestimated the abundance
498 of size classes 4 and 5 for northern shrimp (Fig. 7).

499 **DISCUSSION**

500 Managed populations exhibit heterogeneous and complex spatial structure, which is often
501 overlooked in modeling their population dynamics for management and conservation (Turner et
502 al. 1995, Goethel et al. 2011, Crone 2016). Here, we developed a size-structured spatiotemporal
503 model for estimating fine spatial scale population dynamics and anthropogenic impacts, i.e.,
504 fishery dynamics, and used two marine invertebrates with different types of life history to
505 demonstrate our modeling approach. The spatiotemporal model produced unbiased estimates of
506 abundance and fishing mortality spatially and outperformed a spatially-implicit model when time-
507 varying selectivity caused by spatial heterogeneity in fishing pressure is ignored. To our
508 knowledge, this is the first study to use a simulation experiment to compare the performance of
509 spatially-explicit and spatially-implicit models that include fishery harvest. Our modeling
510 approach bridges the gap between species distribution and population dynamic models and
511 provides the opportunity to improve natural resource management and conservation by explicitly
512 modeling species' spatiotemporal population and anthropogenic dynamics.

513 We have demonstrated that our modeling framework can be adapted to populations with
514 different types of life history through straightforward modifications to the population dynamic
515 component, i.e., $g(\mathbf{n}_{s,t})$. Although we presented a size-structured model, it is fairly easy to modify
516 $g(\mathbf{n}_{s,t})$ to an age-structured model. The modeling framework is also flexible enough to
517 accommodate varying degrees of model complexity. In the simplest scenario, the number of
518 size/age classes can be reduced to one and the population dynamic component can be modified to
519 be a delay-difference (Thorson et al. 2015) or biomass dynamic model (Thorson et al. 2017a).
520 Furthermore, environmental covariates, e.g., sea surface/bottom temperature, salinity, and etc., can
521 be easily incorporated in the model. Hypotheses such as environmentally-driven recruitment,
522 impact of habitat loss and climate change, and climate change-related distribution shifts can be
523 examined directly within the modeling framework at a fine spatial scale, which may be more useful
524 than approaches that treat model estimates as data for subsequent analysis and rely upon spatially-
525 aggregated data. Finally, movement can be explicitly incorporated to the model as we did in the
526 OM. The movement function in the OM accounts for both diffusive and advective movement
527 patterns. However, the simulation scenarios we tested in this study only have diffusive movement.
528 Future research could seek to evaluate different movement patterns, e.g., ontogenetic movement. It
529 is common for aquatic and terrestrial animals to have movement patterns varying with ontogeny.
530 For example, older birds with more experience are more likely to innovate new migration patterns
531 in response to global change (Teitelbaum et al. 2016).

532 Integral projection models (IPMs), which predict vital rates from state variables (e.g., size,
533 weight, or age) and covariates (e.g., environment) using regression models, have been increasingly
534 applied to animal and plant populations (e.g., Coulson et al. 2010, Jongejans et al. 2011, Coulson
535 2012, Merow et al. 2014). These models are considered to have strengths compared to traditional

536 matrix population models (Merow et al. 2014). However, spatial heterogeneity, as one of the most
537 important factors influencing population dynamics, is much less often incorporated into IPMs.
538 Crone (2016) found that spatial heterogeneity increased population growth rates of pasqueflower
539 and suggests that it is important to consider spatial heterogeneity when modeling plant population
540 dynamics. Research efforts have been made to link IPMs with dispersal to model spatial spread
541 (Jongejans et al. 2011). We envision that the similar spatiotemporal modelling approach as we
542 proposed here could be an interesting avenue for future research of IPMs.

543 Spatially-explicit population dynamics models are increasingly structured using multiple
544 spatial strata (Goethel et al. 2011, Goethel and Berger 2017). However, this approach requires
545 extensive data to allow a fine spatial scale because (1) each stratum needs sufficient data so that
546 model is tractable, and (2) additional data are needed to estimate or predefine the connectivity
547 among strata, e.g., movement. As a result, such models are rarely concurrently or historically used
548 across the entire assessment-management interface, due to the need for quantifiable data. However,
549 our modeling framework relies upon totally different structure and assumption, i.e., population
550 density is continuous across the whole area, and estimates the density fields based on geostatistical
551 theory. Therefore, spatial-referenced data from fishery-independent and -dependent survey can be
552 directly used in the model. Based on our simulation experiment on sample size, we consider that
553 many species which have been surveyed routinely have adequate data to fit this model. Few studies
554 have been conducted to investigate this approach (Kristensen et al. 2014, Thorson et al. 2015).
555 Kristensen et al. (2014) demonstrates that it is feasible to combine stock assessment and
556 spatiotemporal dynamics. However, they did not include the fisheries processes in their model.
557 Thorson et al. (2015) used a similar modeling approach to estimate a spatially-explicit delay-
558 difference dynamic of a fish population. Our study is an extension of these two and provides a

559 more general modeling framework and rigorous model evaluation. Spatiotemporal models can also
560 be used as operating models for conducting management strategy evaluation (Boyd et al. 2018),
561 evaluating the performance of stock assessment models, and optimizing sampling design.

562 Spatially-stratified models do not always outperform spatially-implicit models (Szwarczak
563 and Punt 2015). In some cases, spatially-implicit models are more robust than spatially-stratified
564 models, especially when there is uncertainty in population spatial structure (e.g., mis-specified
565 spatial strata) and movement. However, the spatiotemporal model of this paper does not rely on
566 spatial strata and accounts for movement implicitly without requiring additional data. Based on
567 our simulation study, we also found that when there is no complex spatial structure, spatially-
568 implicit model had similar performance as the spatiotemporal model in estimating spatially-
569 aggregated population and fishery quantities. The comparison scenario we show here represents
570 the situation where a strong and persistent gradient of fishing pressure occurs over space and time.
571 In this case, a spatially-implicit model could not accurately estimate the population-level fishing
572 mortality. Similar results have been found in Sampson et al. (2011) where an age-structured model
573 was used. Therefore, we envision that our spatiotemporal modeling approach would be especially
574 useful for species that have protected areas or where population pressures vary substantially across
575 space. For instance, spatially-explicit population models have been used to evaluate habitat
576 restoration for cactus wren (*Campylorhynchus brunneicapillus sandiegensis*) (Conlisk et al. 2014).
577 Also, spatiotemporal models can be used to determine the abundance and spatial pattern for
578 endangered species such as amur tiger (*Panthera tigris altaica*) and leopard (*Panthera pardus*
579 *orientalis*) (Wang et al. 2016) so that effective conservation plans can be developed.

580 We showed that the spatiotemporal model outperforms spatially-implicit model due to its
581 ability to attribute changes in selectivity to spatial patterns in fishery exploitation. Specifically, the

582 spatially-implicit model assumed that fishery selectivity was constant over time, and this
583 specification was a poor approximation to fishery removals. It is well known that misspecification
584 of selectivity would lead to biased estimates of population quantities (Linton and Bence 2011,
585 Stewart and Martell 2014), and some fishery stock assessments specify time-varying selectivity
586 (Martell and Stewart 2014). Therefore, spatially-implicit models that estimate time-varying
587 selectivity may produce less biased results e.g., using time-varying selectivity and accounting for
588 autocorrelation among size and time (Xu et al. 2018). However, this approach to time-varying
589 selectivity requires estimating a process (aggregate fishery selectivity) that cannot be corroborated
590 through any field sampling, whereas the spatio-temporal model used here approximates the same
591 process by estimating spatial variation in population density, and we argue that the latter is superior
592 because (1) it is more biologically interpretable and (2) could be corroborated by other field
593 sampling.

594 We conclude that spatially-explicit population models can provide valuable insights into
595 population dynamics and spatial distribution that are not possible with either spatially-implicit
596 models or species distribution models in isolation, and are useful tools for population ecologists,
597 conservation biologists, and land managers. This advance comes at the expense of greater data
598 requirements. However, we argue that, when there are survey demographic data available, it can
599 be advantageous to investigate size-structured spatiotemporal models.

600 ACKNOWLEDGEMENTS

601 We thank K. Kristensen and the developers of Template Model Builder, without which this
602 analysis would not be feasible. J. Cao was supported by NOAA “Stock Assessment and Analytic
603 Methods” (SAAM) grant awarded in 2016 to J. Thorson, A. Punt, and C. Szuwalski. This
604 publication is funded by the Joint Institute for the Study of the Atmosphere and Ocean (JISAO)

- 605 under NOAA Cooperative Agreement NA15OAR4320063, Contribution No XXX. We thank R.
- 606 Methot for helpful comments on an earlier draft.

For Review Only

607 **REFERENCES**

- 608 Abbott, J. K., B. Garber-Yonts, and J. E. Wilen. 2010. Employment and Remuneration Effects of
609 IFQs in the Bering Sea/Aleutian Islands Crab Fisheries. *Marine Resource Economics*
610 25:333–354.
- 611 Adams, L. G., R. O. Stephenson, B. W. Dale, R. T. Ahgook, and D. J. Demma. 2008. Population
612 Dynamics and Harvest Characteristics of Wolves in the Central Brooks Range, Alaska.
613 *Wildlife Monographs* 170:1–25.
- 614 Benson, A. J., S. P. Cox, and J. S. Cleary. 2015. Evaluating the conservation risks of aggregate
615 harvest management in a spatially-structured herring fishery. *Fisheries Research* 167:101–
616 113.
- 617 Berkeley, S. A., M. A. Hixon, R. J. Larson, and M. S. Love. 2004. Fisheries Sustainability via
618 Protection of Age Structure and Spatial Distribution of Fish Populations. *Fisheries* 29:23–
619 32.
- 620 Beverton, R. J. H., and S. J. Holt. 1957. On the Dynamics of Exploited Fish Populations.
621 Investigat. U.K. Ministry of Agriculture and Fisheries, London.
- 622 Bieber, C., and T. Ruf. 2005. Population dynamics in wild boar *Sus scrofa* : ecology, elasticity of
623 growth rate and implications for the management of pulsed resource consumers. *Journal of*
624 *Applied Ecology* 42:1203–1213.
- 625 Boudreau, S. A., N. L. Shackell, S. Carson, and C. E. den Heyer. 2017. Connectivity,
626 persistence, and loss of high abundance areas of a recovering marine fish population in the

- 627 Northwest Atlantic Ocean. *Ecology and Evolution* 7:9739–9749.
- 628 Boyd, R., S. Roy, R. Sibly, R. Thorpe, and K. Hyder. 2018. A general approach to incorporating
629 spatial and temporal variation in individual-based models of fish populations with
630 application to Atlantic mackerel. *Ecological Modelling* 382:9–17.
- 631 Cao, J., Y. Chen, and R. A. Richards. 2017. Improving assessment of *Pandalus* stocks using a
632 seasonal, size-structured assessment model with environmental variables. Part II: Model
633 evaluation and simulation. *Canadian Journal of Fisheries and Aquatic Sciences* 74:363–376.
- 634 Chandler, R. B., and J. D. Clark. 2014. Spatially explicit integrated population models. *Methods*
635 in *Ecology and Evolution* 5:1351–1360.
- 636 Chandler, R., and J. Hepinstall-Cymerman. 2016. Estimating the spatial scales of landscape
637 effects on abundance. *Landscape Ecology* 31:1383–1394.
- 638 Conlisk, E., S. Motheral, R. Chung, C. Wisinski, and B. Endress. 2014. Using spatially-explicit
639 population models to evaluate habitat restoration plans for the San Diego cactus wren
640 (*Campylorhynchus brunneicapillus sandiegensis*). *Biological Conservation* 175:42–51.
- 641 Conroy, M. J., Y. Cohen, F. C. James, Y. G. Matsinos, and B. A. Maurer. 1995. Parameter
642 Estimation, Reliability, and Model Improvement for Spatially Explicit Models of Animal
643 Populations. *Ecological Applications* 5:17–19.
- 644 Coulson, T. 2012. Integral projections models, their construction and use in posing hypotheses in
645 ecology. *Oikos* 121:1337–1350.
- 646 Coulson, T., S. Tuljapurkar, and D. Z. Childs. 2010. Using evolutionary demography to link life

- 647 history theory, quantitative genetics and population ecology. *Journal of Animal Ecology*
- 648 79:1226–1240.
- 649 Cressie, N., C. A. Calder, J. S. Clark, J. M. Ver Hoef, and C. K. Wikle. 2009. Accounting for
650 uncertainty in ecological analysis: the strengths and limitations of hierarchical statistical
651 modeling. *Ecological Applications* 19:553–570.
- 652 Crone, E. E. 2016. Contrasting effects of spatial heterogeneity and environmental stochasticity
653 on population dynamics of a perennial wildflower. *Journal of Ecology* 104:281–291.
- 654 Dunning, J. B., D. J. Stewart, B. J. Danielson, B. R. Noon, T. L. Root, R. H. Lamberson, and E.
655 E. Stevens. 1995. Spatially Explicit Population Models: Current Forms and Future Uses.
656 *Ecological Applications* 5:3–11.
- 657 Ehrlén, J., and W. F. Morris. 2015. Predicting changes in the distribution and abundance of
658 species under environmental change. *Ecology Letters* 18:303–314.
- 659 Elith, J., and J. R. Leathwick. 2009. Species Distribution Models: Ecological Explanation and
660 Prediction Across Space and Time. *Annual Review of Ecology, Evolution, and Systematics*
661 40:677–697.
- 662 Goethel, D. R., and A. M. Berger. 2017. Accounting for spatial complexities in the calculation of
663 biological reference points: effects of misdiagnosing population structure for stock status
664 indicators. *Canadian Journal of Fisheries and Aquatic Sciences* 74:1878–1894.
- 665 Goethel, D. R., C. M. Legault, and S. X. Cadrian. 2015. Testing the performance of a spatially
666 explicit tag-integrated stock assessment model of yellowtail flounder (*Limanda*

- 667 *ferruginea*) through simulation analysis. Canadian Journal of Fisheries and Aquatic
668 Sciences 72:582–601.
- 669 Goethel, D. R., T. J. Quinn, and S. X. Cadrin. 2011. Incorporating Spatial Structure in Stock
670 Assessment: Movement Modeling in Marine Fish Population Dynamics. Reviews in
671 Fisheries Science 19:119–136.
- 672 Guisan, A., T. C. Edwards, and T. Hastie. 2002. Generalized linear and generalized additive
673 models in studies of species distributions: setting the scene. Ecological Modelling 157:89–
674 100.
- 675 Jongejans, E., K. Shea, O. Skarpaas, D. Kelly, and S. P. Ellner. 2011. Importance of individual
676 and environmental variation for invasive species spread: a spatial integral projection model.
677 Ecology 92:86–97.
- 678 Jongejans, E., O. Skarpaas, and K. Shea. 2008. Dispersal, demography and spatial population
679 models for conservation and control management. Perspectives in Plant Ecology, Evolution
680 and Systematics 9:153–170.
- 681 Kareiva, P., A. Mullen, and R. Southwood. 1990. Population Dynamics in Spatially Complex
682 Environments: Theory and Data. Philosophical Transactions of the Royal Society B:
683 Biological Sciences 330:175–190.
- 684 Krebs, C. J. 1972. Ecology : the experimental analysis of distribution and abundance.
685 HarperCollins College Publishers, New York, NY.
- 686 Kristensen, K., A. Nielsen, C. W. Berg, H. Skaug, and B. Bell. 2015. TMB: automatic

- 687 differentiation and Laplace approximation. arXiv preprint arXiv:1509.00660.
- 688 Kristensen, K., U. H. Thygesen, K. H. Andersen, and J. E. Beyer. 2014. Estimating spatio-
689 temporal dynamics of size-structured populations. Canadian Journal of Fisheries and
690 Aquatic Sciences 71:326–336.
- 691 Kuo, T.-C., S. Mandal, A. Yamauchi, and C. Hsieh. 2015. Life history traits and exploitation
692 affect the spatial mean-variance relationship in fish abundance. Ecology 97:15–1270.1.
- 693 Lee, H.-H., K. R. Piner, M. N. Maunder, I. G. Taylor, and R. D. Methot. 2017. Evaluation of
694 alternative modelling approaches to account for spatial effects due to age-based movement.
695 Canadian Journal of Fisheries and Aquatic Sciences 74:1832–1844.
- 696 Linton, B. C., and J. R. Bence. 2011. Catch-at-age assessment in the face of time-varying
697 selectivity. ICES Journal of Marine Science 68:611–625.
- 698 Martell, S., and I. Stewart. 2014. Towards defining good practices for modeling time-varying
699 selectivity. Fisheries Research 158:84–95.
- 700 Maunder, M. N., and K. R. Piner. 2015. Contemporary fisheries stock assessment: many issues
701 still remain. ICES Journal of Marine Science 72:7–18.
- 702 Merow, C., J. P. Dahlgren, C. J. E. Metcalf, D. Z. Childs, M. E. K. Evans, E. Jongejans, S.
703 Record, M. Rees, R. Salguero-Gómez, and S. M. McMahon. 2014. Advancing population
704 ecology with integral projection models: a practical guide. Methods in Ecology and
705 Evolution 5:99–110.
- 706 Mueter, F. J., and M. A. Litzow. 2008. Sea ice retreat alters the biogeography of the Bering Sea

- 707 continental shelf. *Ecological Applications* 18:309–320.
- 708 Okubo, A., and S. A. Levin. 1989. A Theoretical Framework for Data Analysis of Wind
709 Dispersal of Seeds and Pollen. *Ecology* 70:329–338.
- 710 Parada, C., D. A. Armstrong, B. Ernst, S. Hinckley, and J. M. Orensanz. 2010. Spatial dynamics
711 of snow crab (*Chionoecetes opilio*) in the eastern Bering Sea—putting together the pieces of
712 the puzzle. *Bulletin of Marine Science* 86:413–437.
- 713 Phillips, S. J., R. P. Anderson, M. Dudík, R. E. Schapire, and M. E. Blair. 2017. Opening the
714 black box: an open-source release of Maxent. *Ecography* 40:887–893.
- 715 Punt, A. E., M. Haddon, L. R. Little, and G. N. Tuck. 2016. Can a spatially-structured stock
716 assessment address uncertainty due to closed areas? A case study based on pink ling in
717 Australia. *Fisheries Research* 175:10–23.
- 718 Punt, A. E., M. Haddon, and G. N. Tuck. 2015. Which assessment configurations perform best in
719 the face of spatial heterogeneity in fishing mortality, growth and recruitment? A case study
720 based on pink ling in Australia. *Fisheries Research* 168:85–99.
- 721 Sampson, D. B., and R. D. Scott. 2011. A spatial model for fishery age-selection at the
722 population level. *Canadian Journal of Fisheries and Aquatic Sciences* 68:1077–1086.
- 723 Sampson, D. B., and R. D. Scott. 2012. An exploration of the shapes and stability of population-
724 selection curves. *Fish and Fisheries* 13:89–104.
- 725 Sampson, D. B., R. D. Scott, and T. Quinn. 2011. A spatial model for fishery age-selection at the
726 population level. *Canadian Journal of Fisheries and Aquatic Sciences* 68:1077–1086.

- 727 Sippel, T., J. Paige Eveson, B. Galuardi, C. Lam, S. Hoyle, M. Maunder, P. Kleiber, F. Carvalho,
728 V. Tsontos, S. L. H. Teo, A. Aires-da-Silva, and S. Nicol. 2015. Using movement data from
729 electronic tags in fisheries stock assessment: A review of models, technology and
730 experimental design. *Fisheries Research* 163:152–160.
- 731 Stewart, I. J., and S. J. D. Martell. 2014. A historical review of selectivity approaches and
732 retrospective patterns in the Pacific halibut stock assessment. *Fisheries Research* 158:40–49.
- 733 Szuwalski, C. S., and A. E. Punt. 2015. Can an aggregate assessment reflect the dynamics of a
734 spatially structured stock? Snow crab in the eastern Bering Sea as a case study. *Fisheries
735 Research* 164:135–142.
- 736 Teitelbaum, C. S., S. J. Converse, W. F. Fagan, K. Böhning-Gaese, R. B. O'Hara, A. E. Lacy,
737 and T. Mueller. 2016. Experience drives innovation of new migration patterns of whooping
738 cranes in response to global change. *Nature Communications* 7:12793.
- 739 Thorson, J. T. 2017. Three problems with the conventional delta-model for biomass sampling
740 data, and a computationally efficient alternative. *Canadian Journal of Fisheries and Aquatic
741 Sciences*.
- 742 Thorson, J. T., and M. A. Haltuch. 2018. Spatio-temporal analysis of compositional data:
743 increased precision and improved workflow using model-based inputs to stock assessment.
744 *Canadian Journal of Fisheries and Aquatic Sciences:cjfas-2018-0015*.
- 745 Thorson, J. T., J. N. Ianelli, S. B. Munch, K. Ono, and P. D. Spencer. 2015. Spatial delay-
746 difference models for estimating spatiotemporal variation in juvenile production and
747 population abundance. *Canadian Journal of Fisheries and Aquatic Sciences* 72:1897–1915.

- 748 Thorson, J. T., J. Jannot, and K. Somers. 2017a. Using spatio-temporal models of population
749 growth and movement to monitor overlap between human impacts and fish populations.
750 Journal of Applied Ecology 54:577–587.
- 751 Thorson, J. T., S. B. Munch, J. M. Cope, and J. Gao. 2017b. Predicting life history parameters
752 for all fishes worldwide. Ecological Applications 27:2262–2276.
- 753 Thorson, J. T., S. B. Munch, and D. P. Swain. 2017c. Estimating partial regulation in
754 spatiotemporal models of community dynamics. Ecology 98:1277–1289.
- 755 Turner, M. G., G. J. Arthaud, R. T. Engstrom, S. J. Hejl, J. Liu, S. Loeb, and K. McKelvey.
756 1995. Usefulness of Spatially Explicit Population Models in Land Management. Ecological
757 Applications 5:12–16.
- 758 Wang, T., L. Feng, P. Mou, J. Wu, J. L. D. Smith, W. Xiao, H. Yang, H. Dou, X. Zhao, Y.
759 Cheng, B. Zhou, H. Wu, L. Zhang, Y. Tian, Q. Guo, X. Kou, X. Han, D. G. Miquelle, C. D.
760 Oliver, R. Xu, and J. Ge. 2016. Amur tigers and leopards returning to China: direct
761 evidence and a landscape conservation plan. Landscape Ecology 31:491–503.
- 762 Xu, H., J. T. Thorson, R. D. Methot, and I. G. Taylor. 2018. A new semi-parametric method for
763 autocorrelated age- and time-varying selectivity in age-structured assessment models.
764 Canadian Journal of Fisheries and Aquatic Sciences:cjfas-2017-0446.
- 765
- 766

767 Table 1. List of indices used in model descriptions, data used during parameter estimation and
 768 simulation, and all parameters (the type of each parameter is listed as estimated (“fixed”,
 769 “random”), or calculated from estimated parameters (“derived quantity”)).
 770

Name	Symbol	Type
Sample	i	Index
Location	s	Index
Year	t	Index
Size bin	l	Index
Immaturity	ω	index
Maturity	λ	index
Knot	j	Index
Number of years	τ	Index
Data of i th sample at location s and time t	$x(s_i, t_i)$	Data
Area swept for sample i	a_i	Data
Maturity at size	\mathbf{w}	Data
Sex ratio of the recruits (male)	p^{male}	Data
Growth transition matrix	\mathbf{G}	Data
Natural mortality at size	\mathbf{m}	Data
Movement matrix	\mathbf{M}	Data
Biomass per group of individuals	$\delta(s_i, t_i)$	Data/derived quantity
Biomass	b	Data/derived quantity
Number of animals	n	Data/derived quantity
Encounter probability	p	Derived quantity
Recruitment at size for location s and year t	$\mathbf{r}_{s,t}$	Derived quantity
Selectivity at size	\mathbf{v}	Derived quantity
Catch at size for location s and year t	$\mathbf{c}_{s,t}$	Derived quantity
Aggregate selectivity for size class l and year t	$s_{l,t}$	Derived quantity
Variance of positive catch rate	σ_D^2	Parameter (fixed)
Initial abundance at size	Φ	Parameter (fixed)
Variance of fishing mortality	σ_f^2	Parameter (fixed)
Logistic selectivity parameter	θ	Parameter (fixed)
Logistic selectivity parameter	l_{50}	Parameter (fixed)
Average recruitment of year t	r_t	Parameter (fixed)
Pairwise covariance between any two size classes	Θ_L	Parameter (fixed)
Decorrelation distance	κ	Parameter (fixed)
Matérn smoothness parameter	ν	Parameter (fixed)
Process error for year t	\mathbf{E}_t	Parameter (random)
Observation-level random effect	η_i	Parameter (random)
Fully-selected fishing mortality at location s	\mathbf{f}_s	Parameter (random)
Abundance at size over time	\mathbf{N}	Parameter (random)

771
 772

773 Table 2. The average Root-Mean-Square Error (RMSE) and Relative Bias (RB) of estimated
 774 abundance-at-size for northern shrimp and snow crab in data poor, moderate and rich scenarios.
 775

size class	sample size	Northern shrimp		Snow crab	
		RMSE (%)	RB (%)	RMSE (%)	RB (%)
1	50	6.13	-0.9077	4.08	-1.0498
1	100	3.95	-0.6968	3.21	-1.2290
1	200	2.67	-0.5925	2.24	-0.7661
2	50	5.87	-0.1665	4.02	-0.7559
2	100	3.65	-0.3300	2.94	-0.5656
2	200	2.58	-0.2433	2.17	-0.5143
3	50	6.13	0.3595	3.51	-0.3060
3	100	3.77	0.0082	2.48	-0.2885
3	200	2.56	-0.0809	2.02	-0.2478
4	50	6.31	3.0897	3.61	0.5006
4	100	3.84	1.6495	2.59	0.1132
4	200	2.61	0.8710	1.92	0.0059
5	50	6.19	2.4945	3.58	0.4051
5	100	4.26	1.4511	2.53	0.1206
5	200	3.40	0.9986	2.00	0.0917

776
 777

778 **FIGURES**

779

780 Figure 1. Comparison of simulated and estimated distribution of size classes 1, 3 and 5 in selected
781 years using data without measurement error and movement (experiment 1). Warm colors indicate
782 high values, and cool colors indicate low values.

783

784 Figure 2. Comparison of simulated (red line) and estimated (black dot) spatially-aggregated total
785 abundance (a) and total removals (b) by size class over time for the scenario with no measurement
786 error nor movement (experiment 1). 95% confidence intervals ($\pm 1.96 \times SE$, where SE is the
787 estimated standard error) are shown using error bars.

788

789 Figure 3. Comparison of simulated (red line) and estimated (black dot) spatially-aggregated total
790 abundance (a) and total removals (b) by size class over time for the stochastic data scenario with
791 movement (a randomly selected replicate) (experiment 1). 95% confidence intervals ($\pm 1.96 \times SE$,
792 where SE is the estimated standard error) are shown by error bars. Standard deviations used when
793 generating data are 0.5 for both survey and fishery catches.

794

795 Figure 4. The relative errors (percentages) of abundance-at-size estimated from spatially-implicit
796 and spatiotemporal models (experiment 2). Median Root-mean-square error (RMSE) and relative
797 bias (RB) in percentage across years are listed in each panel for comparison.

798

799 Figure 5. The relative errors (percentages) of total abundance and spawning stock biomass from
800 the spatially-implicit and spatiotemporal models (experiment 2).

801

802 Figure 6. The true population-level selectivity at size $s_{l,t}$ (defined in Eq. 21, black dotted line) and
803 95 percentiles of the estimated selectivity at size from the spatially-implicit model (red) and
804 spatiotemporal model (yellow) over 50 replicates (experiment 2).

805

806 Figure 7. Boxplot of Root-Mean-Square Error (RMSE) and Relative Bias (RB) of abundance-at-
807 size across replicates for data poor, moderate and rich scenarios, for northern shrimp and snow
808 crab (experiment 3).

809

For Review Only

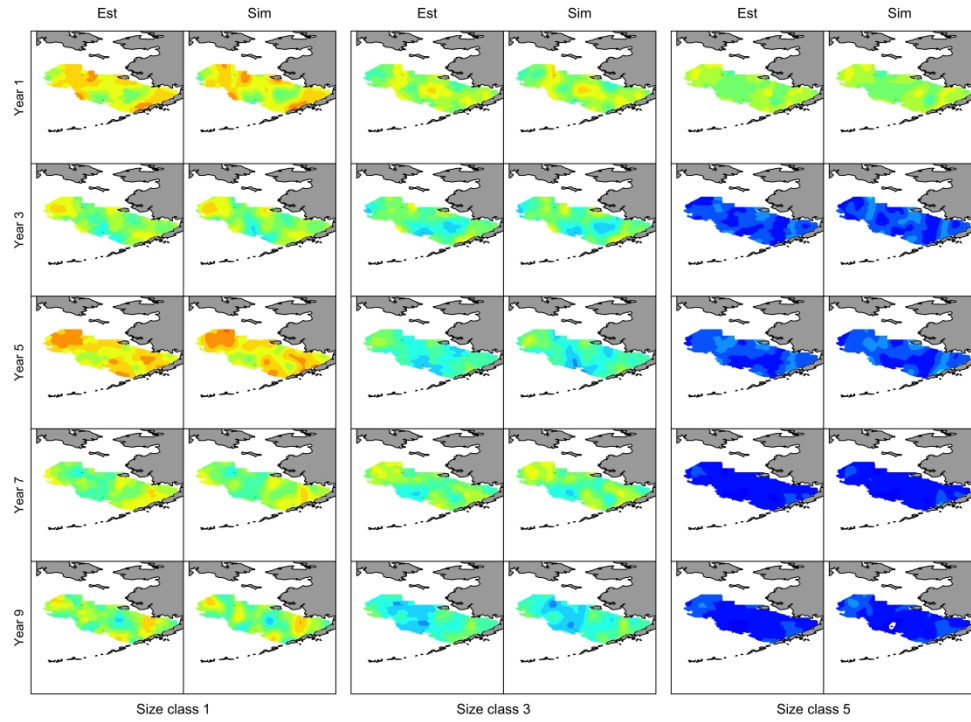
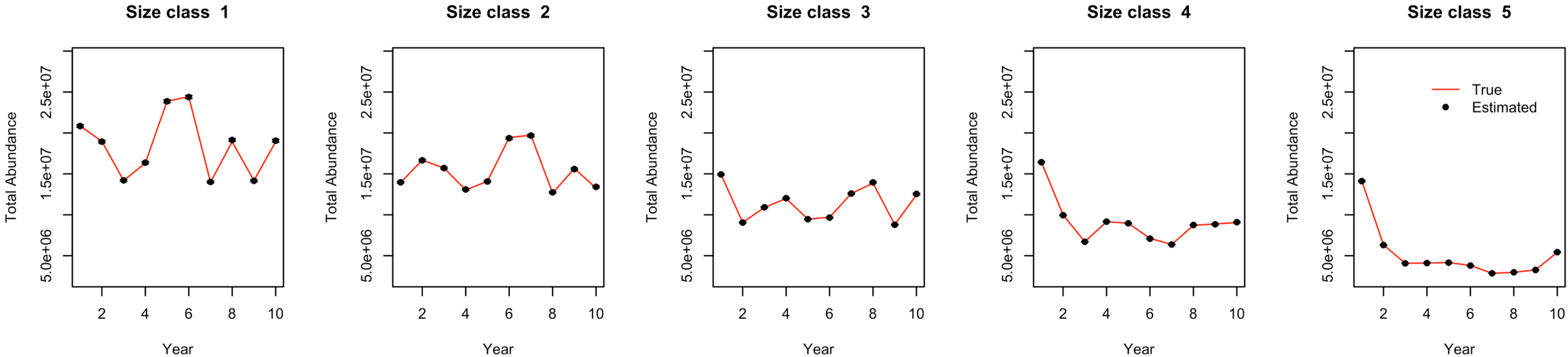


Figure 1. Comparison of simulated and estimated distribution of size classes 1, 3 and 5 in selected years using data without measurement error and movement (experiment 1). Warm colors indicate high values, and cool colors indicate low values.

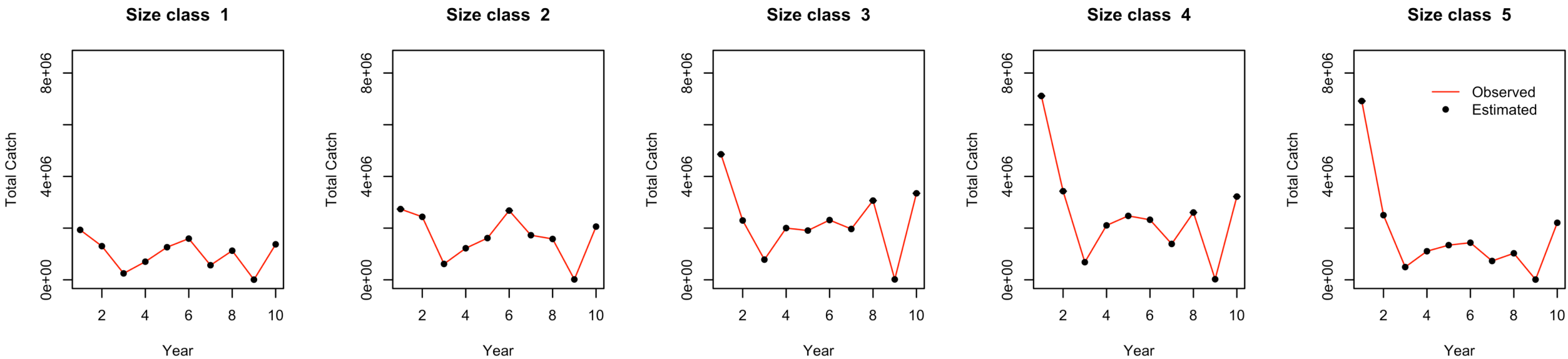
2540x1905mm (72 x 72 DPI)

Fish and Fisheries

(a)



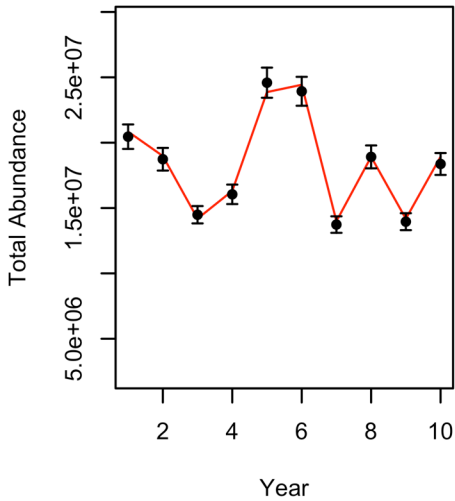
(b)



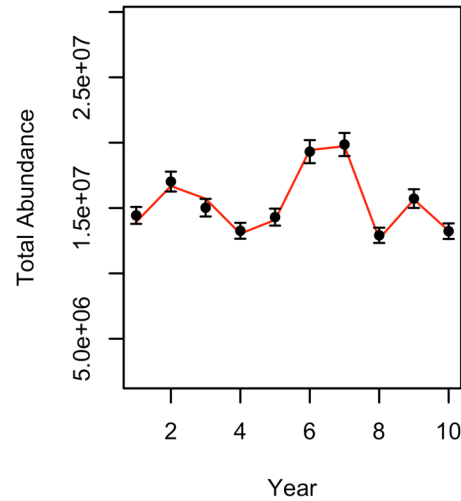
Fish and Fisheries

(a)

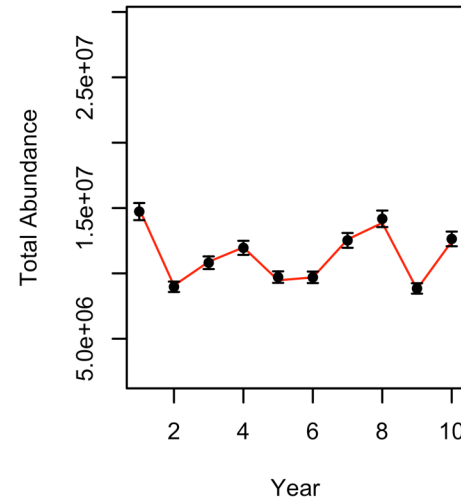
Size class 1



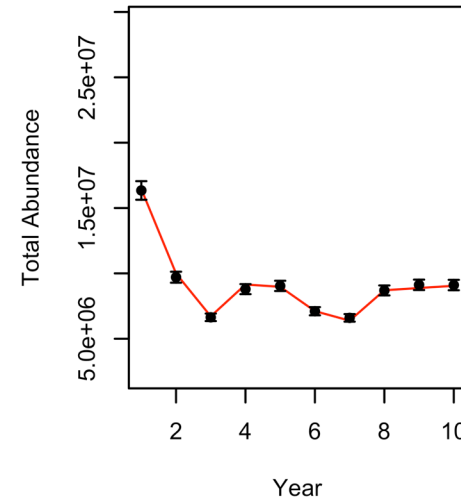
Size class 2



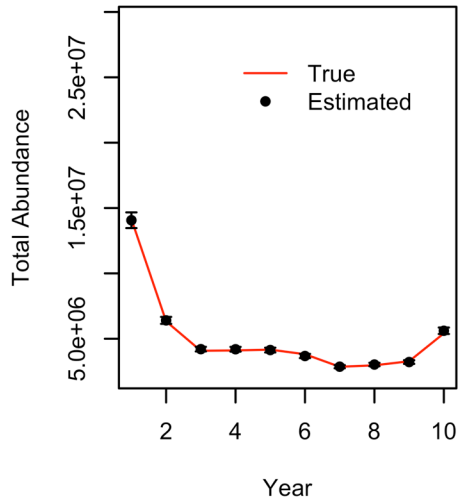
Size class 3



Size class 4

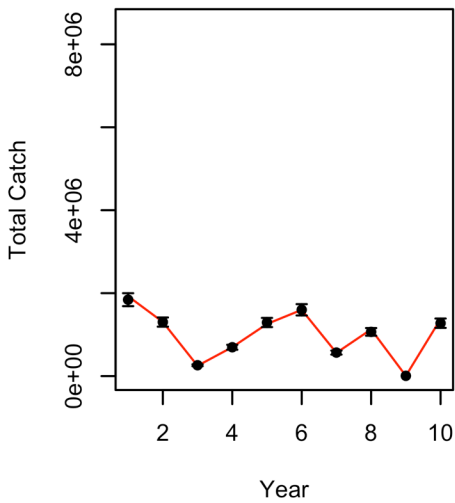


Size class 5

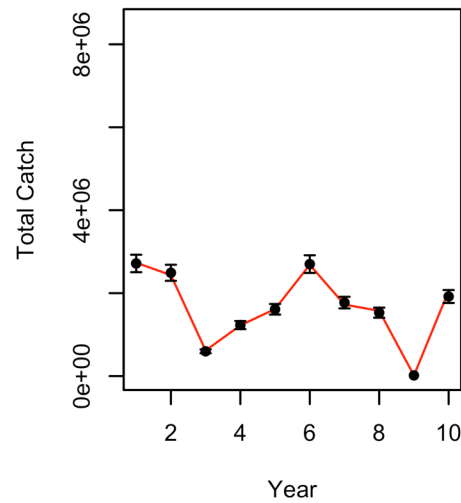


(b)

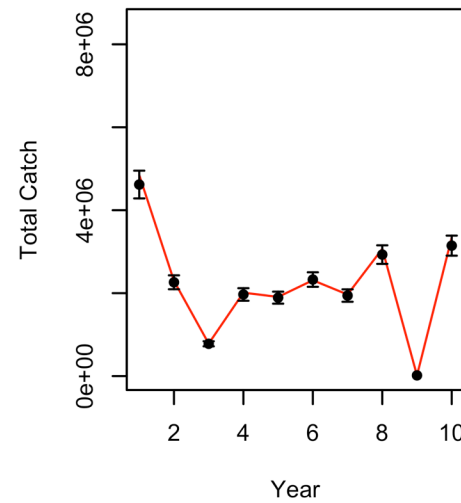
Size class 1



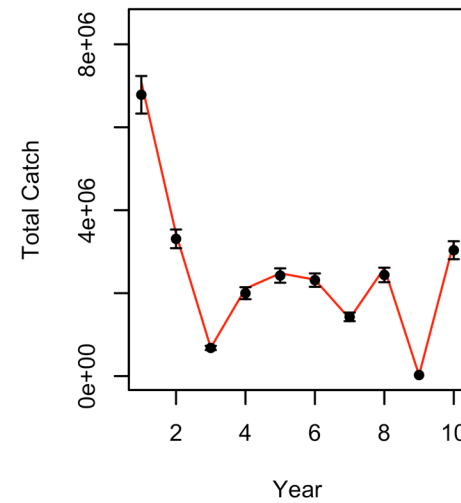
Size class 2



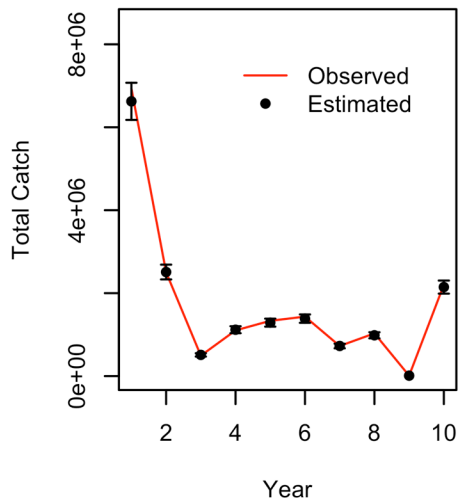
Size class 3



Size class 4



Size class 5



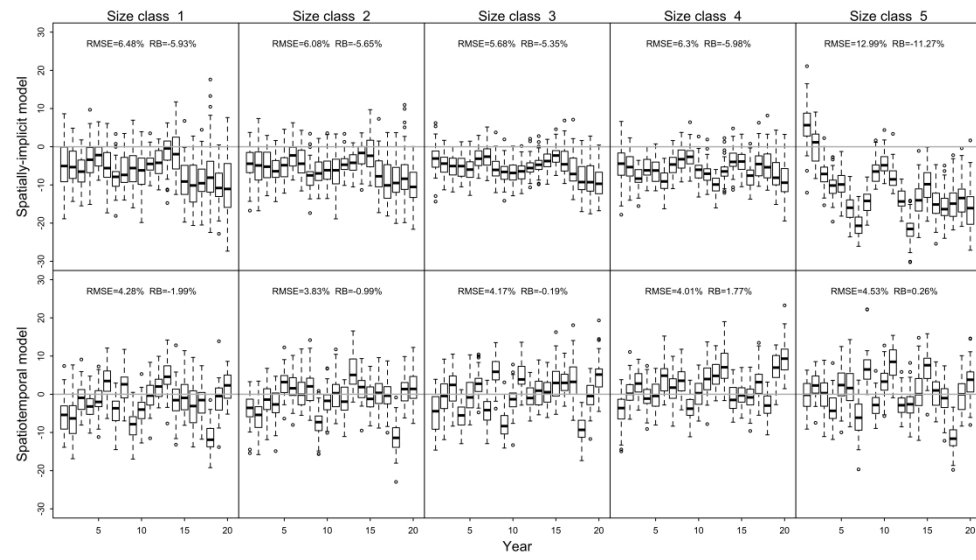


Figure 4. The relative errors (percentages) of abundance-at-size estimated from spatially-implicit and spatiotemporal models (experiment 2). Median Root-mean-square error (RMSE) and relative bias (RB) in percentage across years are listed in each panel for comparison.

2540x1481mm (72 x 72 DPI)

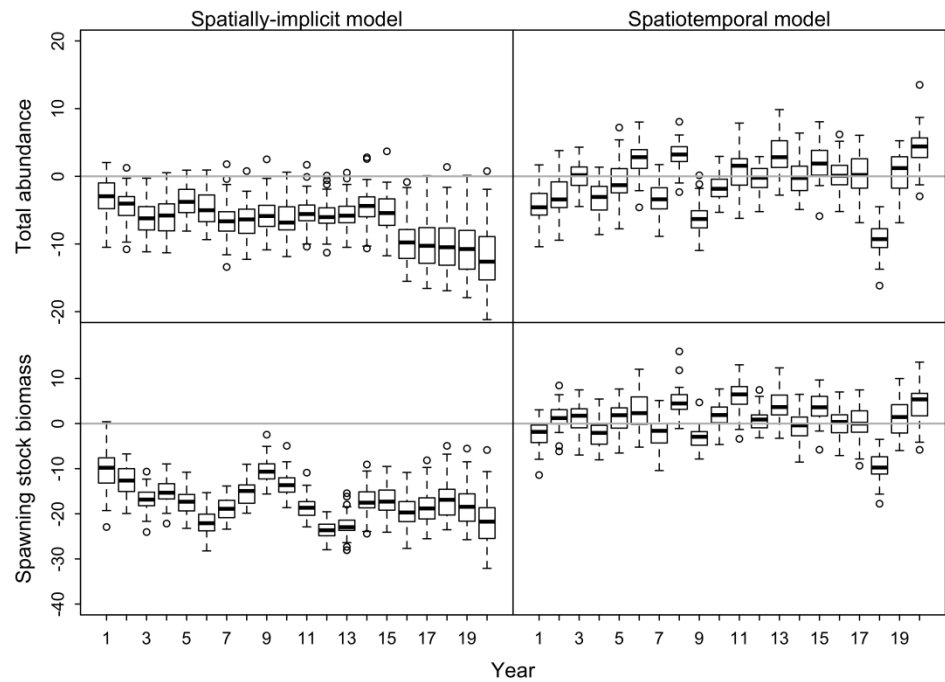


Figure 5. The relative errors (percentages) of total abundance and spawning stock biomass from the spatially-implicit and spatiotemporal models (experiment 2).

1693x1270mm (72 x 72 DPI)

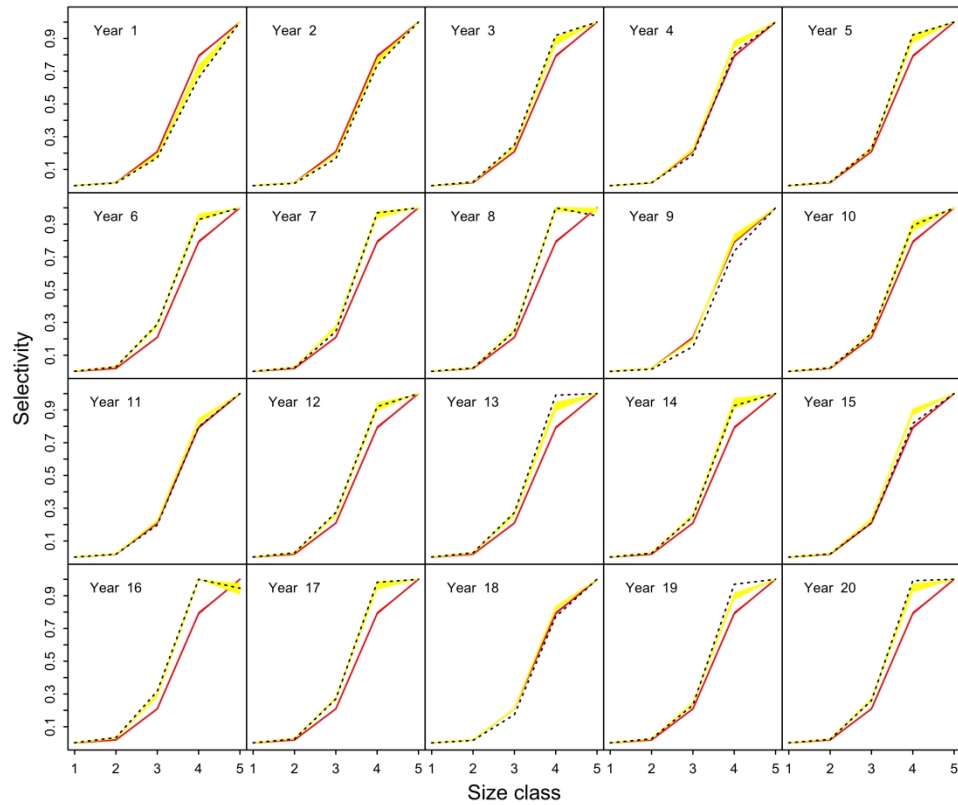


Figure 6. The true population-level selectivity at size $s_{(l,t)}$ (defined in Eq. 21, black dotted line) and 95 percentiles of the estimated selectivity at size from the spatially-implicit model (red) and spatiotemporal model (yellow) over 50 replicates (experiment 2).

1693x1481mm (72 x 72 DPI)

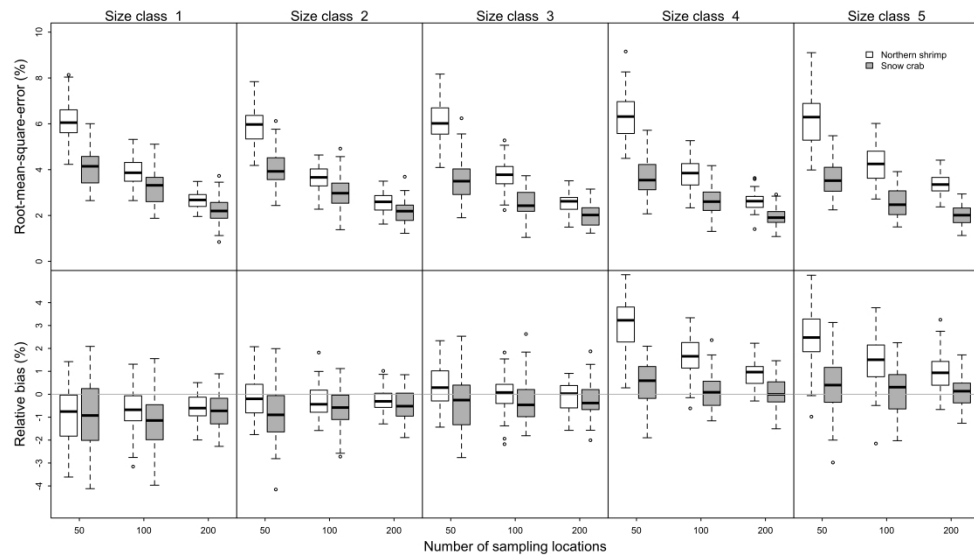


Figure 7. Boxplot of Root-Mean-Square Error (RMSE) and Relative Bias (RB) of abundance-at-size across replicates for data poor, moderate and rich scenarios, for northern shrimp and snow crab (experiment 3).

2540x1481mm (72 x 72 DPI)

1 Appendix 1: Movement matrix calculation on the grids

2 We represent movement in a vector-matrix form as:

$$3 \quad \frac{\partial}{\partial t} \mathbf{n} = \mathbf{N} \mathbf{n} \quad (\text{A1})$$

4 where \mathbf{N} is the matrix of instantaneous movement rates. \mathbf{N} is a sparse matrix, in which most of the
 5 elements are zeros, and element n_{r_1, r_2} is nonzero only if grids r_1 and r_2 share the same edge. This
 6 is biologically reasonable because crab can only move to adjacent grids in any instant. \mathbf{N} is non-
 7 symmetric because n_{r_1, r_2} and n_{r_2, r_1} represent the instantaneous movement rate from grid r_2 to
 8 grid r_1 and the opposite direction, respectively. \mathbf{N} is decomposed into movement in each of four
 9 cardinal directions, $\mathbf{N}_{east}, \mathbf{N}_{north}, \mathbf{N}_{west}, \mathbf{N}_{south}$.

$$10 \quad \mathbf{N} = m_1 \mathbf{N}_{east} + m_2 \mathbf{N}_{north} + m_3 \mathbf{N}_{west} + m_4 \mathbf{N}_{south} \quad (\text{A2})$$

11 where m_1 , m_2 , m_3 , and m_4 represent the magnitude of movement in each cardinal direction. In
12 this study, we assume $m_1 = m_2 = m_3 = m_4$ (only diffusion but not advection). The diagonal of \mathbf{N}
13 is the -1 times the sum of non-zero values of the column, such that each column has sum of zero
14 (representing a conservation of individuals during movement). Calculating the matrix \mathbf{M} of annual
15 movement rates from \mathbf{N} (matrix of instantaneous movement rates) requires matrix exponential
16 operation, which results in a dense \mathbf{M} . Because there are over 36,000 grids in this study, a dense
17 \mathbf{M} would slow down the simulation and require considerable memory. Therefore, the Euler
18 approximation, which can preserve the sparsity of \mathbf{N} , is used to approximate \mathbf{M} :

$$\mathbf{M} \approx \left(\mathbf{I} + \frac{\mathbf{N} \Delta t}{n_{tdiv}} \right)^{n_{tdiv}} \quad (\text{A3})$$

20 where n_{tdiv} is the number of time-steps used when using a difference-equation approximation.
 21 However, as n_{tdiv} is increased, \mathbf{M} becomes denser and the approximation approaches the matrix

22 exponential operation. In this study, n_{tdiv} is set to 10, which is a balance between computational
23 speed and approximation accuracy.

For Review Only

24 **Appendix 2: Procedure to simulate the distribution of recruitment and fishing mortality**

25 Simulating the distribution of recruitment involves the following steps: (1) draw annual
 26 mean recruitments \mathbf{r}_t from a Poisson distribution or define \mathbf{r}_t to have a specific temporal pattern;
 27 (2) simulate a Gaussian random field for each year on the grid (Σ_t^r) based on predefined spatial
 28 variance σ_t^r and scale κ_t^r using *RandomFields* package (Schlather 2009); (3) calculate recruitment
 29 for each cell and year using $\mathbf{R}_{s,t} = \mathbf{r}_t e^{\Sigma_t^r}$; and (4) allocate recruitment $\mathbf{R}_{s,t}$ to each size class. The
 30 distribution of fully-selected fishing mortality is simulated in the similar way ($\mathbf{F}_{s,t} = \mathbf{f}_t e^{\Sigma_t^f}$). The
 31 values used in the simulation are shown in Table A1 for snow crab and Table A2 for northern
 32 shrimp.

33 For northern shrimp, we divided the spatial domain into inshore and offshore areas (A1
 34 and A2; Fig. A7) and simulate the fishing mortality over these two areas separately:

$$35 \quad \mathbf{F}_{s,t} = \begin{cases} \mathbf{f}_{A1,t} e^{\Sigma_t^f} & s \in A1 \\ \mathbf{f}_{A2,t} e^{\Sigma_t^f} & s \in A2 \end{cases}$$

36 where $\mathbf{f}_{A1,t}$ and $\mathbf{f}_{A2,t}$ are the mean fishing mortality of year t for inshore and offshore areas,
 37 respectively. We assume that $\mathbf{f}_{A1,t}$ and $\mathbf{f}_{A2,t}$ have the same temporal trend, but with different
 38 magnitude (i.e., $\mathbf{f}_{A1,t} = 4 \times \mathbf{f}_{A2,t}$). Spatial variance σ_t^f and scale κ_t^f used for these two areas are
 39 the same.

40

41 **Appendix 3: Simulation of sampling process**

42 Sampling errors for survey catch rates and fishery removals are simulated on the grid
 43 spatial scale. For each size class, the observed catch of a randomly selected location and fishery
 44 removal for each grid are simulated from lognormal distribution:

45 $b_{s,t,l} \sim \text{lognormal}(\log(n_{s,t,l}) - \sigma_b^2/2, \sigma_b^2)$

46 $c_{s,t,l}^o \sim \text{lognormal}(\log(c_{s,t,l}) - \sigma_c^2/2, \sigma_c^2)$

47 where σ_b and σ_c are set to 0.3 for both snow crab and northern shrimp cases. We have tried different
 48 values, and the general conclusions are not sensitive to these values.

49 For spatially-implicit model, the input data are aggregated across the area and the
 50 abundance index (b_t) and total catch (c_t^o) are calculated as:

51 $b_t = \frac{\sum_s \sum_L b_{s,t,l}}{n_s}$

52 $c_t^o = \sum_L \sum_{n_r} c_{s,t,l}^o$

53 where n_s and n_r are the number of sampling locations and total grids, respectively. The standard
 54 deviations of the abundance index (σ_b^n) and the total catch (σ_c^n) are assumed known for spatially-
 55 implicit model. The standard deviations of abundance index and total catch are calculated:

56 $\sigma_b^n = \sqrt{\frac{\sum (\sum_L b_{s,t,L} - b_t)^2}{n_s - 1}}$

57 $\sigma_c^n = n_r \sqrt{\frac{\sum (\sum_L c_{s,t,L}^o - c_t^o)^2}{n_r}}$

58 The size compositions of survey ($p_{l,t}^b$) and fishery ($p_{l,t}^c$) are calculated as:

59 $p_{l,t}^b = \frac{\sum_s b_{s,t,l}}{\sum_L \sum_s b_{s,t,l}}$

60

$$p_{l,t}^c = \frac{\sum_{nr} c_{s,t,l}^o}{\sum_L \sum_{nr} c_{s,t,l}^o}$$

61 The input sample size for the spatially-implicit model is set to the number of locations sampled.

For Review Only

62 Table A1.

Item	Descriptor	Note
Years covered	10	Annual time step
Number sexes	1	Male
Lengths	25-125 mm	
Length bins	20 mm	5 size classes
Recruitment length bin	25-45 mm	size class 1
Natural mortality	0.23yr ⁻¹ for all size	constant through space and time
Maturity (male)	Size-specific	$w = c(0,0.05,0.1,0.4,1)$
Growth (male)	intercept = 15; slope = 1.0; beta = 0.1	constant through space and time; growth transition matrix is calculated as: $l_{L+1} = \text{int} + \text{slope} * l_L;$ $P_{L \rightarrow L+1} = \int \text{gamma}(\frac{l_{L+1}}{\text{slope}}, \text{beta});$
Commercial selectivity	Logistic	$\theta = 0.05; l_{50} = 75 \text{ mm}$
Survey	Survey at the start of the year	catchability = 1; selectivity =1 for all size classes
Initial condition		50-year burn-in period
Fishing mortality	$\sigma_t^f=0.2;$ $\kappa_t^f=1.2$	$\log(f_t) \sim \text{Normal}(\log(0.5), 0.2);$ σ_t^f and κ_t^f are constant over time
Recruitment	$\sigma_t^r=0.3;$ $\kappa_t^r=1.5$	$r_t \sim \text{Lognormal}(6.32, 0.3)$ σ_t^r and κ_t^r are constant over time

63

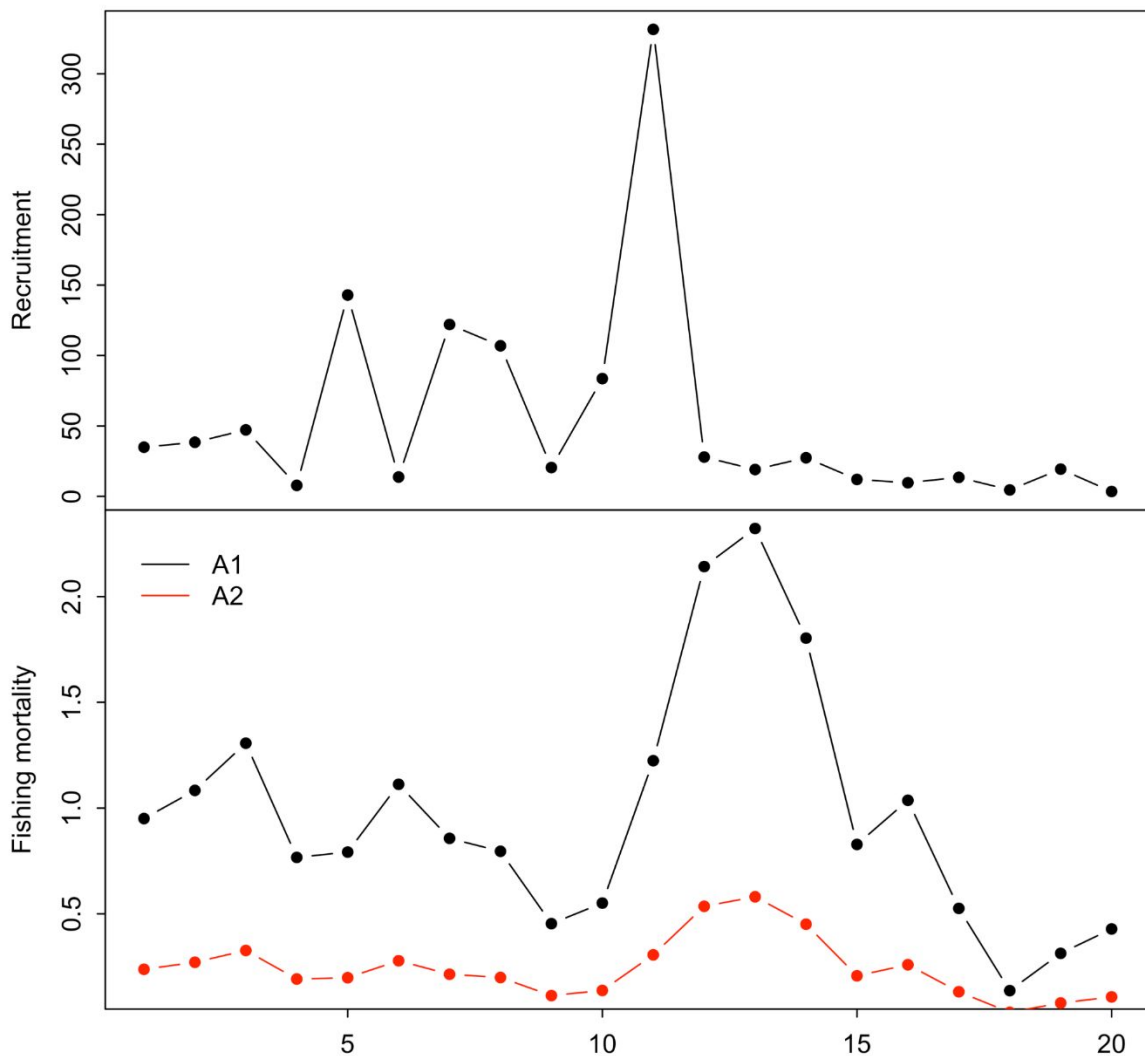
64

65 Table A2.

Item	Descriptor	Note
Years covered	20	Annual time step
Number sexes	1	
Lengths	9-34 mm	
Length bins	5 mm	5 size classes
Recruitment length bin	9-14 mm	size class 1
Natural mortality	0.25yr ⁻¹ for all size	constant through space and time
Growth	$L_{inf} = 35;$ $SD_{Linf} = 1.0;$ $K = 0.2;$ $SD_k = 0.1;$ $\rho_{Linf_K} = 0.9;$	constant through space and time; growth transition matrix is calculated following Chen et al. (2003)
Commercial selectivity	Logistic	$\theta = 0.32; l_{50} = 22.4 \text{ mm}$
Survey	Survey at the start of the year	catchability = 1; selectivity =1 for all size classes
Initial condition		50-year burn-in period
Fishing mortality	$\sigma_t^f=0.3;$ $\kappa_t^f=0.4$	$f_{A1, t}, f_{A2, t}$: Figure A1 σ_t^f and κ_t^f are constant over time
Recruitment	$\sigma_t^r=0.2;$ $\kappa_t^r=0.4$	r_t : Figure A1 σ_t^r and κ_t^r are constant over time

66

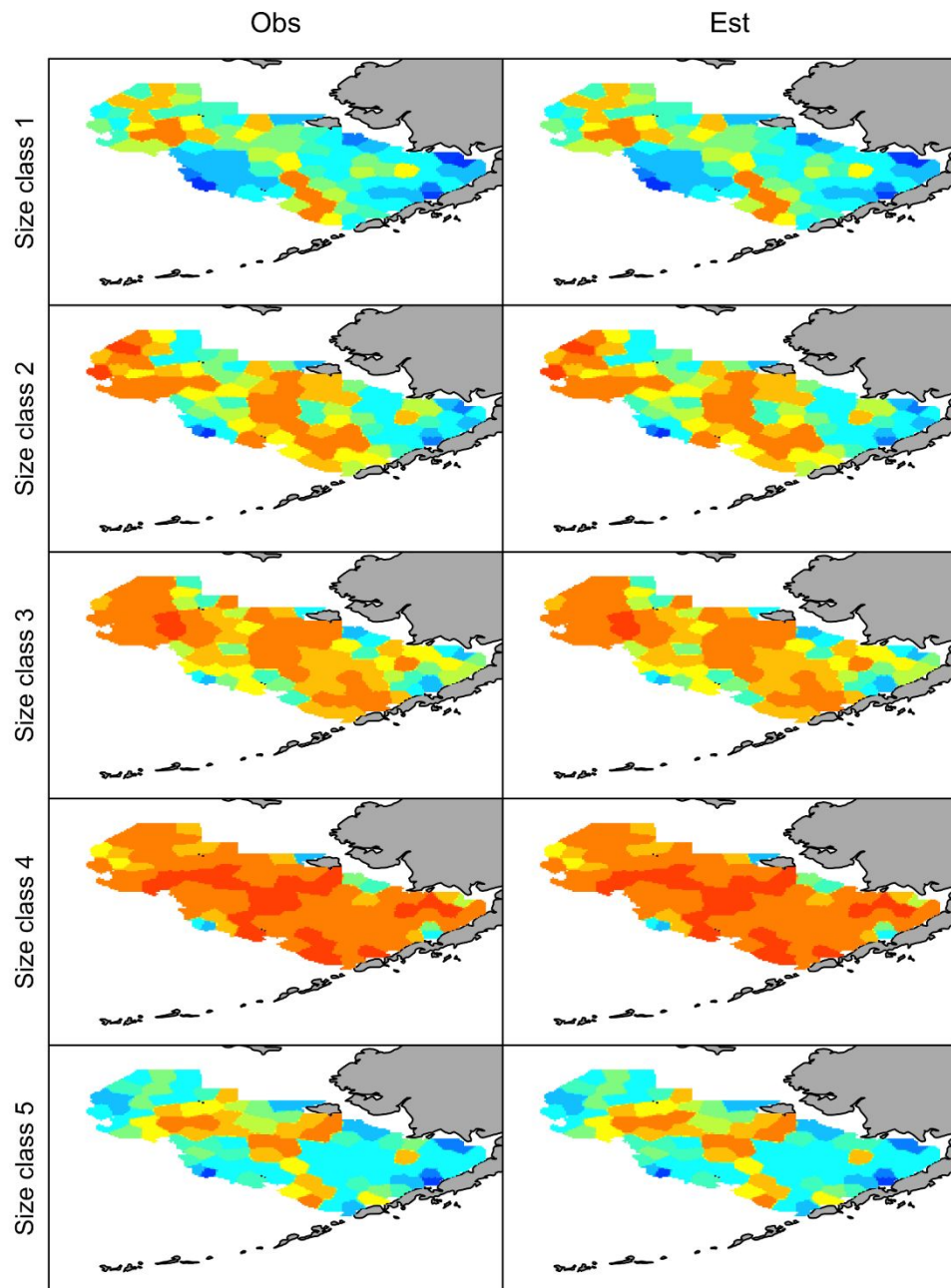
67



68

69 Figure A1. Mean recruitment and fishing mortality over time used in the simulation of northern
70 shrimp population

71



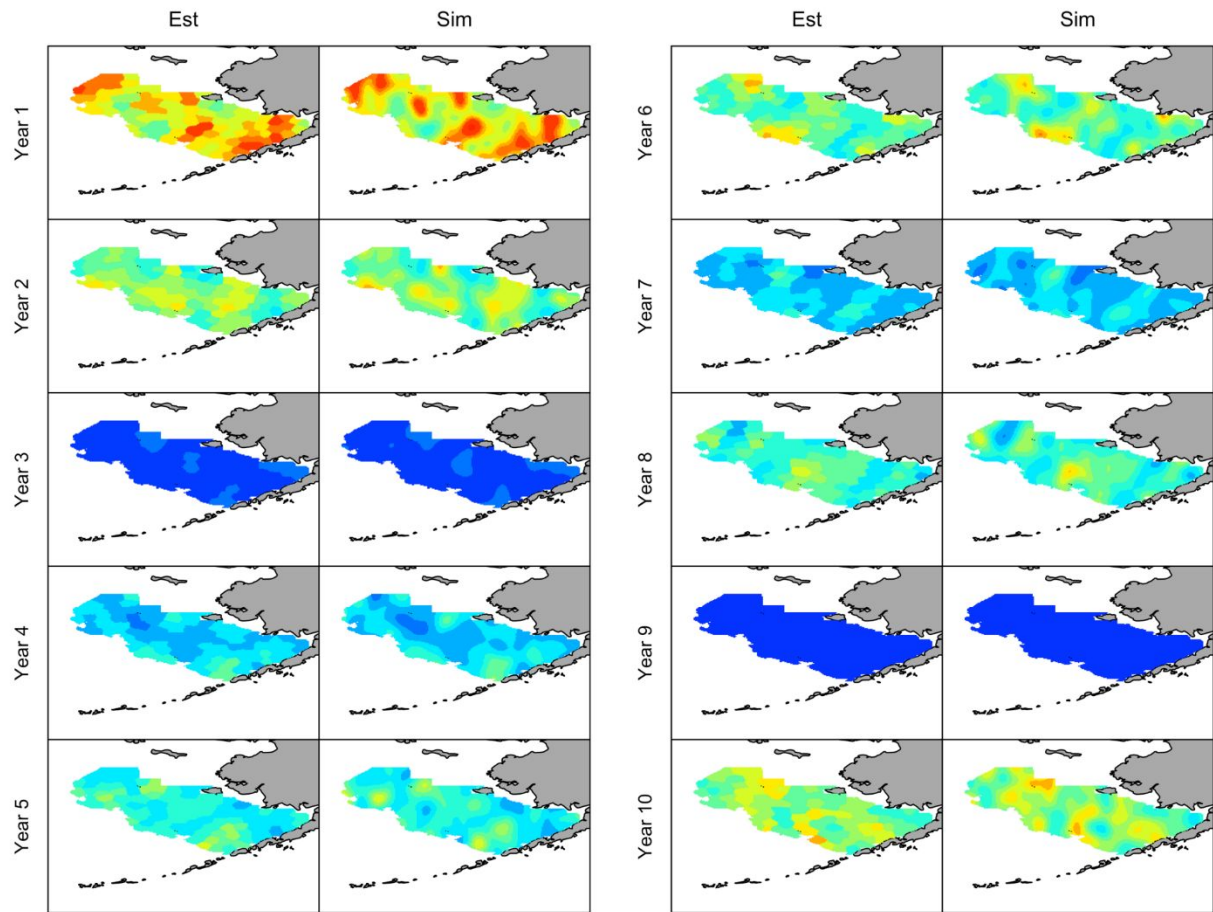
72

73

74 Figure A2. An example of comparison of simulated and estimated distribution of fishery catch for
75 year 5 using data without measurement error. Warm colors indicate high values, and cool colors
76 indicate low values.

77

78



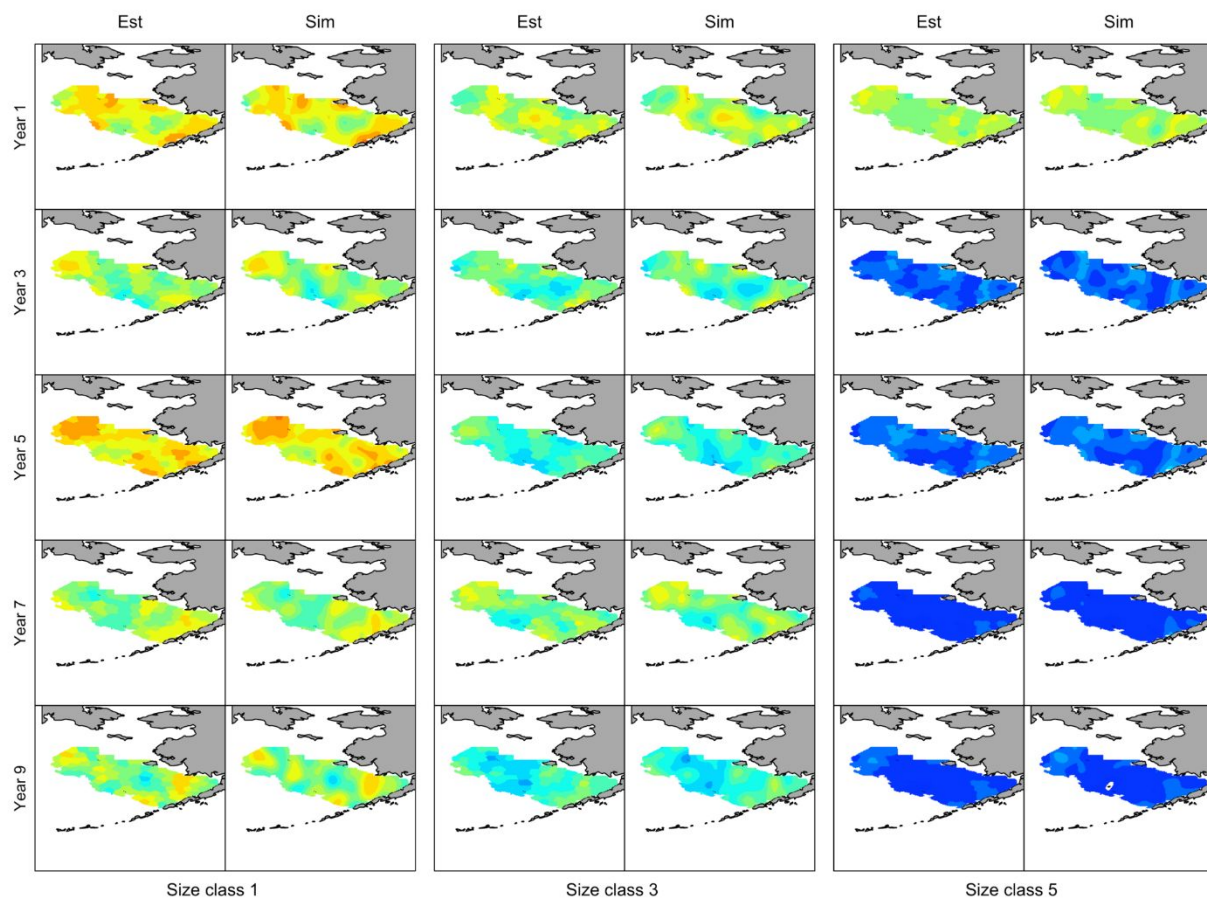
79

80

81 Figure A3. Comparison of simulated and estimated distribution of fully-selected fishing mortality
82 over 10 years for the scenario in which the data have no measurement error (without movement).
83 Warm colors indicate high values, and cool colors indicate low values.

84

85

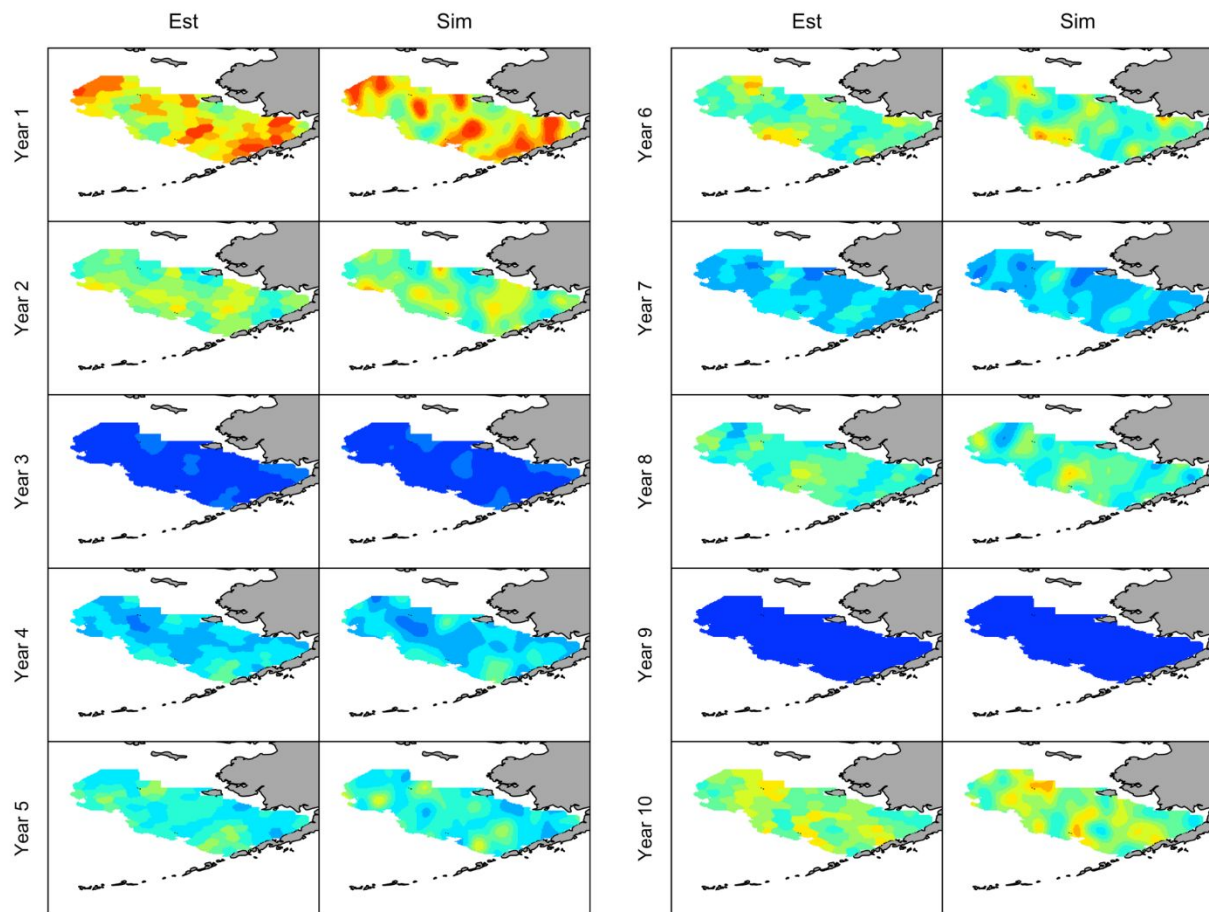


86

87 Figure A4. Comparison of simulated and estimated distribution of size classes 1, 3 and 5 in selected
88 years using data without measurement error (with movement). Warm colors indicate high values,
89 and cool colors indicate low values.

90

91



92

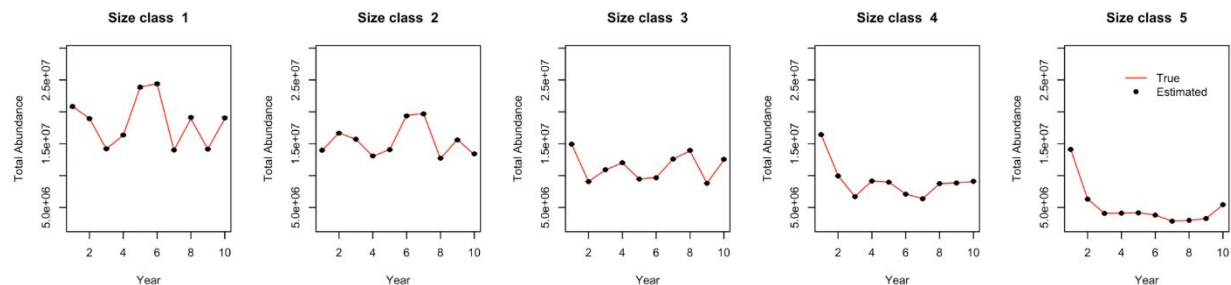
93 Figure A5. Comparison of simulated and estimated distribution of fully selected fishing mortality
94 over 10 years for the scenario in which the data have no measurement error (with movement).

95 Warm colors indicate high values, and cool colors indicate low values.

96

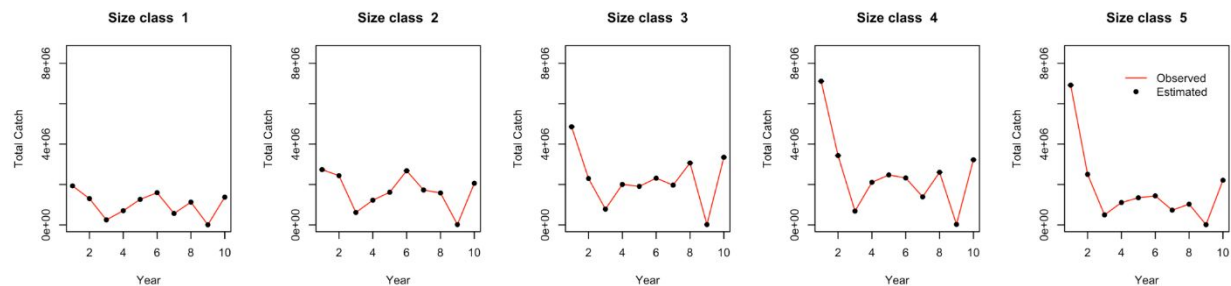
97

98 (a)



99

100 (b)



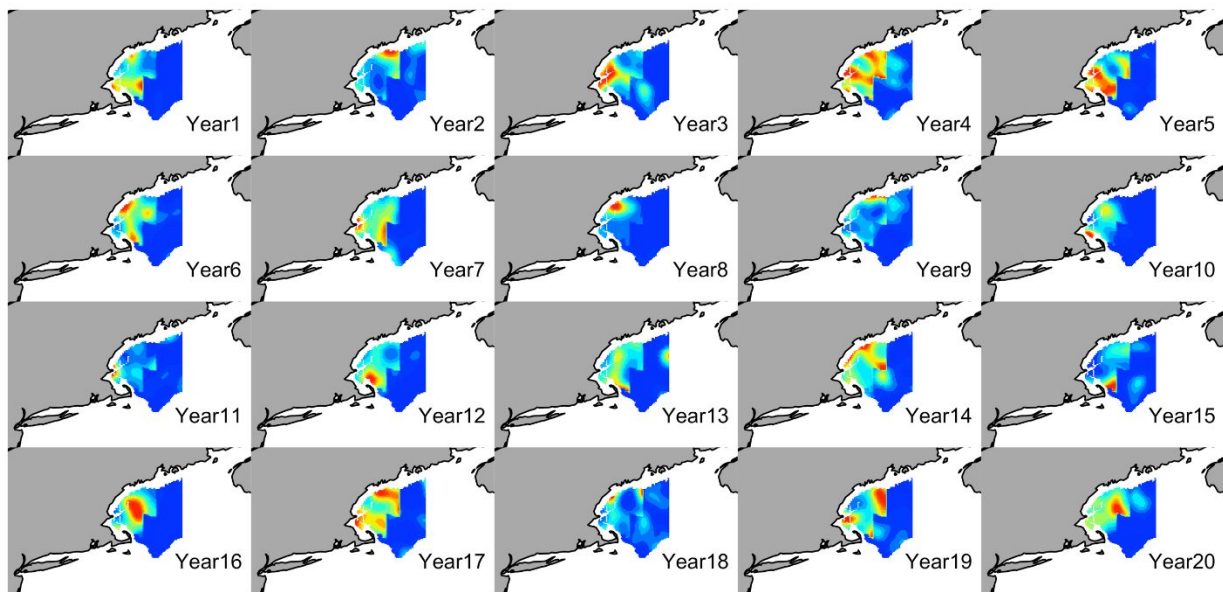
101

102 Figure A6. Comparison of simulated (red line) and estimated (black dot) spatially-aggregated total
 103 abundance (a) and total removals (b) of each size class over time for the scenario in which the data
 104 have no measurement error (with movement). 95% confidence interval ($\pm 1.96 \times \text{SE}$, where SE is
 105 the estimated standard error) shown in error bar.

106

107

108



109

110 Figure A7. Simulated fishing mortality for northern shrimp (inshore area has persistent higher
111 fishing mortality over time than offshore area).

112